Combining Constrained Heptapeptide Cassettes With Computational Design to Create Coiled-coil Targeting Helical Peptides

Alexander Lathbridge[1] and Jody M. Mason[1,2,3]

[1]Dept of Biology and Biochemistry, University of Bath, Claverton Down, Bath BA2 7AY

[2]Centre for Therapeutic Innovation, University of Bath, Claverton Down, Bath BA2 7AY

[3]To whom correspondence should be addressed: j.mason@bath.ac.uk

Running title: Coiled coil targeting peptide cassettes

**Corresponding author: Jody M. Mason (E: j.mason@bath.ac.uk; T: +441225386867)*

Keywords: Coiled coil; Peptide antagonist, peptide cassettes, constrained peptides; heptads; Activator Protein-1; transcription factor.

ABSTRACT

Thirty-two heptapeptides have been synthesized and characterised to establish the effect of Lys→Asp (i→i+4) lactamisation upon their ability to adopt a helical conformation. Since most parallel and dimeric coiled coil sequences can be deconvoluted into ***gabcdef*** repeats, we have introduced fixed solvent exposed b→f (K→D) constraints into this design scaffold. Interfacial ***'a'*** hydrophobic (L/I/V/N) and ***'e/g'*** electrostatic (E/K) options (4 x 2 x 2 = 16 cassettes) were introduced as core drivers of coiled coil stability and specificity. All present as random coil when linear but adopt a helical conformation upon lactamisation. Helicity varied in magnitude from 34% to 68%, indicating different levels of constraint tolerance within the context of a sequence required to be helical for function. Using the oncogenic transcription factor cJun as an exemplar, we next utilised our bCIPA coiled coil screening engine to select four cassettes of highest predicted affinity when paired with four ***gabcdef*** cassettes within the full-length cJun target counterpart (16^4 = 65,536 combinations). This information was coupled with observed helicity for each constrained cassette to select for the best balance of predicted affinity when linear *and* experimentally validated helicity when constrained. As a control, the same approach was taken using cassettes of high predicted target affinity, but with lower experimentally validated helicity. The approach provides a novel platform of modular heptapeptide cassettes experimentally validated and separated by helical content. Appropriate cassettes can be selected and conjugated to produce longer peptides in which constraints impart appropriate helicity such that a wide range of targets can be engaged with high affinity and selectivity.

INTRODUCTION

It is very difficult to establish if a given peptide sequence will tolerate a helix inducing constraint, meaning that their introduction into peptide sequences towards the goal of imparting helicity, and ultimately increased target affinity, is largely a trial-and-error process[1]. However, it has long been known that peptides of less than 15 residues (1-4 helical turns) are unable to independently form thermodynamically stable α-helices in water[2]. Longer helices form due to a sequential development of intra-strand hydrogen bonds, propagating from a N-terminal folding nucleus towards the C-terminus[3]. This process is interrupted within short synthetic sequences as water molecules compete with the C=O:H-N interactions of the peptide backbone, meaning that the formation of the helix becomes energetically less favourable since the entropic cost associated with folding increases[4]. Helical stabilisation of shorter peptides is therefore an area of intense interest, particularly in protein-protein interactions where biological activity is mediated by helicity[5]. Multiple methods to modify peptides to increase their stability have been explored, including hydrogen bond surrogates[6,7], triazole linkers[8], hydrocarbon staples[4], double-click linkers[9,10], lactam bridges[2,9–12], and other techniques based on macrocyclisation chemistries.[9,10]

Of all helix-inducing constraints currently available, lactamisation is a particularly powerful approach to increasing the stability of short helical peptides. It is an example of side-chain stapling, in which, for example, a peptide bond can be formed between Lys and Asp residues. By coupling amine and carboxylate containing side chains at residues spaced 4 residues apart (i-i+4 configuration) the constraint is able to function such as to complement that of the hydrogen bonds found in native α-helices[4,5,9,13]. Although successful lactamisation of small peptides has been observed[11,14–17] there is still a lack of comparative data on tolerance with respect to longer peptide sequences, and consequent designs that can be implemented towards practical usage. Our group have adopted a strategy of K→D lactamisation, since this has been shown to be the most potent inducer of α-helicity in short peptide sequences relative to alternative approaches[2] .

Here we describe a technique that combines computational design[18–22] with single heptad lactamisation to form stable and functional coiled coil peptides. We are primarily focused on the comparison of i→i+4 (K→D) lactamisation tolerance within individual heptad cassettes corresponding to coiled coil sequences. This is towards a major goal of increasing helicity conferred upon parental sequences in which heptad repeats are contained, thus avoiding a trial and error search for constraints that will be tolerated or that, more importantly, will impart helicity. We are additionally interested in combining the most promising lactamised heptads to form longer peptides in which they are tolerated. Previous studies of helicity imposed by lactamisation of pentapeptides have shown that this has the potential to be used as a generalised approach[12]. We have previously demonstrated the *bZIP*

Coiled coil Interaction Prediction Algorithm (bCIPA) to be a valuable tool in the design of peptides that can antagonise coiled coil interactions involved in the formation of basic leucine zippers (bZIPs)[18,21,22]. Here we describe the combination of computational and experimental techniques towards investigating the ability to generate helically constrained heptads. These are then applied towards the larger goal of designing longer constrained α-helices in which the likelihood of achieving increased helicity and more importantly, improved binding, is increased. As a proof of concept, we explore the ability of modular heptapeptide cassettes that are capable of interfering with the native cJun coiled coil, relative to a counterpart that despite computational selection, contains heptapeptide modules that are found to constrain poorly. Specifically, we seek to address: ***i)*** does lactamisation promote helicity in heptapeptide cassette sequences? ***ii)*** does the helicity imparted in any given cassette vary according to the sequence? ***iii)*** are cassettes are able to be conjugated into longer sequences while retaining/improving helicity relative to linear counterparts? ***iv)*** Using an exemplar target, can such sequences be used to promote increased target-affinity relative to their linear counterparts?

RESULTS AND DISCUSSION

There are a range of methodologies for constraining short peptides into helical structures, but the most potent inducer of helicity for short sequences has been shown to be K→D (i→i+4) lactamisation[15,23]. Lactamisation has the added benefit of introducing a very discreet change to the linear peptide sequence; the constraint consists simply of a condensation reaction between two naturally occurring side chain sequences, resulting in the formation of a peptide bond. Despite this, for a given sequence it can be very difficult to predict if a lactam bridge will be tolerated, meaning that the process of introducing lactam bridges to impart increased helicity upon is trial and error. Here we describe the first use of an approach that seeks to synthesize and characterise modular cassettes with a wide range of sequence-specific properties that are desired for coiled coil forming interactions, such that they can be sorted into i) those of experimentally validated high helicity and ii) those predicted to bind to an oncongenic coiled coil target sequence. The study provides the first set of modular cassettes that can serve such a purpose, with a view to being able to select the most appropriate balance of helicity and target affinity, such that cassettes can be conjugated towards targeting the cJun coiled coil target.

Heptad Library Design – We have created a peptide library consisting of seven residue sequences that correspond to one heptad repeat of a coiled coil motif (***gabcde***; ***ga***KAL***e***D). In this library, positions ***g*** and ***e*** positions, which are important in forming electrostatic contacts within a coiled coil sequence[24,25] were randomised to generate E/K options, with a view to generating potential attractive and repulsive options with the corresponding positions of the target. Similarly, the ***a*** position corresponding to the core region within a coiled coil sequence was randomised to generate L/I/V/N options. The ***c*** and ***d*** positions were fixed as A and L respectively, to impart helicity and further core hydrophobicity that is characteristic of the parallel dimeric coiled coil motif[26]. Each peptide was next synthesized in both linear and lactamised form (b→f; K→D), to probe for constraint tolerance and helical induction (Figure 1). The options for each cassette therefore provided a library of 16 constrained (***g***/***a***/***e*** options; 2 x 4 x 2 = 16) and 16 linear heptapeptides with diverse electrostatic and hydrophobic characteristics. The options were provided to create a series of modular peptides, generating the required electrostatic and hydrophobic contributions to binding with any heptad counterpart within a defined target helix. In particular, by confining electrostatic interactions between peptide and target (i.e. $g_i - e_{i'+1}$) to the same ***gabcdef*** repeat, interactions could be calculated completely independently during prediction and therefore each cassette considered truly modular. The final two solvent exposed positions (***b*** and ***f;*** i→i+4 spacing) were chosen as the most appropriate positions to constrain within each modular cassette while avoiding potential interference with the binding interface.

Individual Cassette Helicity Measurements – Having synthesized all sixteen peptides as both linear and constrained cassettes (see Figure S1-S4 for mass spectrometry data) it was next sought to establish the extent to which each adopted a helical conformation upon introduction of the lactam constraint (Figure 2). As expected, all sixteen sequences adopted a random coil confirmation in the absence of a lactam constraint, with one characteristic minimum at ~190 nm. In contrast, all sixteen cassettes adopted an α-helical conformation upon introduction of the K→D constraint, with characteristic minima at 208 and 222 nm. However, the extent to which each of the sixteen constrained cassettes adopted a helical conformation varied widely, with values ranging from 34 % to 68 % helicity (eq 1). The helicity of peptides in both linear and constrained format were next studied to establish the fractional helicity (fH) gained in constrained form (Figure 3). In doing so it was found that no cassette in linear form exceeded 19% fH based on the raw 222 nm signal (Figure S5, Table 1), whereas even the lowest lactamised peptide was 34% helical, while displaying a characteristic α-helical signature (Table 1, Figure 3, Figure S6). As all cassettes exhibited helicity at 20°C when lactamised, with further thermal scans undertaken to monitor the stability of the cassettes at 10°C increments. At the final scan of 90°C, although loss of stability for all lactamised cassettes was observed, all 16 presented an α -helical signature with an average of 38% helicity, indicating that

helicity is maintained at higher temperatures where no structure would be expected for any linear counterpart. Constrained peptides displayed characteristic 222/208 minima, and consistent with lactamisation no cooperative unfolding profile was observed. Moreover, after heating to 90°C each cassette returned to within 5% of the original signal when incubated at 20°C (Figure S6), indicating that any loss of structure is fully reversible.

Predicting the Stability of Cassettes with Heptads within cJun – To provide further evidence for the validity of our approach, in parallel to measuring individual cassette helicities, we used bCIPA to screen each of the sixteen sequences against individual ***gabcdef*** heptads within a cJun coiled coil target sequence. This was performed to provide a qualitative ranking of the most appropriate cassette to take forward when only considered as a linear heptad. bCIPA prediction is a useful as a tool to gain understanding of the most appropriate core and electrostatic options required for target stability, as well as for specificity of interaction, for instance in avoiding homodimerization over target interaction[20–22]. Hence, bCIPA aids in selecting which cassettes are most appropriate for conjugation in targeting a coiled coil sequence (i.e which are predicted to bind ***and*** adopt a conformation of high helicity). These can then be taken forward for each given heptad within a target sequence. Since bCIPA is trained and validated on longer coiled coil sequences, the values generated are purely qualitative and are not treated as true T_m values. As shown in Table 2, the bCIPA values generated have been normalised to serve alongside helicity in predicting the most appropriate balance of helicity and affinity for each heptad within the target.

Combinational Design to Target cJun – Two four-heptad peptides were created to target the coiled coil region of the oncogenic transcriptional regulator protein cJun. Using this approach, cassettes were selected that when conjugated in linear form that were predicted to bind with high affinity to the cJun target sequence (Figure 4). In particular, two peptides were tested; one was predicted to contain cassettes that constrain poorly and therefore impart poor helicity upon the full-length peptide sequences (peptide 6-2-13-5; individual cassette fH values = 36%, 34%, 47%, and 41% respectively – Table 2 highlighted in yellow), and a second peptide that was predicted to contain cassettes which constrain well and impart high levels of helicity upon the full-length peptide sequence (peptide 1-3-16-17; individual cassette fH values = 45%, 60%, 55%, and 68% respectively – Table 2 highlighted in green). Both peptides were selected by using a combination of ***i)*** normalised bCIPA values and ***ii)*** the fH of the lactamised cassettes (Table 2). Having calculated fH for all 16 lactamised cassettes, each were next individually screened against the first four heptads of cJun. This permitted selection from 16^4 (65,536) possible unique cassette arrangements to predict the most appropriate sequence for effective binding. Combining cassettes 1, 3, 16, and 7 (Figure 4) led to the design of a constrained

peptide predicted to form both a stable α-helix (average cassette helicity = 57%) but with the additional possibility of forming a higher affinity coiled coil with the target cJun, relative to the linear counterpart (linear 1-3-16-7:cJun bCIPA predicted T_m = 38°C). As a control, cassettes were also conjugated which were similarly highly ranked according to the bCIPA screening process. However, in contrast, these sequences were experimentally validated to be of low isolated helicity (average helicity = 39%, linear 6-2-13-5:cJun bCIPA predicted T_m = 41°C). This resulted in a combination of cassettes 6,2,13, and 5 (Figure 4). This permitted the comparison of two sequences, both of which were predicted to engage with the target as linear 28mers (Figure 4). Computationally, both peptides score very highly, with 6-2-13-5 computationally ranked as #145 and 1-3-16-7 as #450 – both within the top 1% of the library of full length peptides. Indeed, both sequences contain the same net favourable electrostatic contribution (see below), and comparable core contributions, as well as Asn residues at position ***a3*** to promote asymmetric side chain-side chain hydrogen bonding with the corresponding Asn in the cJun partner strand[26,27]. However, while 1-3-16-7 was expected to lactamase well and translate into improved binding, 6-2-13-5 was expected to lactamase poorly leading to a lower gain of coiled coil stability. During the design process eight unique cassettes were selected to avoid duplication of any modules, and to widen the potential understanding of each cassette use in combination. Both sequences 1-3-16-7 (YEIKALED–ELKALED–KNKALKD–EIKALKD) and 6-2-13-5 (YKVKALED–KIKALED–ENKALED–EVKALED) were synthesized with a Tyr at the N-terminus for quantification by UV absorbance. Both sequences terminate at the f position of the 4th heptad (Figure 4), and contained two lactam bridges – one at either termini. As helicity is thought to propagate from the N-terminus to the C-terminus[3], stabilisation via heptads 1 and 4 was predicted to promote overall helicity towards heptads 2 and 3 at the helix interior. In contrast to previous work[18,21,22,28], the 29-mers were not capped with helicity promoting residues (AS at N-terminus and GAP at the C-terminus) to further probe the effect of lactamisation in directly promoting helicity.

Upon inspection of the helical wheels (Figure 4), a pattern of electrostatically favourable and unfavourable interactions was observed. As selected by bCIPA, as a potential homodimer peptide 1-3-16-7 displayed 6 repulsive electrostatic interactions (4 Glu-Glu and 2 Lys-Lys) and only 2 attractive interactions (2 Glu-Lys). In the 6-2-13-5 control, 4 repulsive and 4 attractive interactions are present. As potential heterodimers with cJun, both peptides contain 4 favourable and one unfavourable interaction. As discussed previously[22], cJun contains Gln and Ala at the ***g3*** and ***e3*** positions. The ***a3-a3'*** was chosen to generate an Asn-Asn interaction for both sequences, due to the favourable effect of this interaction on specificity and on the oligomeric state.

Structural Stability of Terminally Lactamised Peptides - An analysis of the global secondary structure of the full-length linear and lactamised peptides was conducted, both in isolation and in complex with with cJun. CD spectra showed 1-3-16-7 to display high levels of helicity in both linear (65.3%) and lactamised (71.4%) forms (Figure 5a). At 20°C, the stability of the two are comparable (ΔfH = 6.1%), with the lactamised version displaying an improved helical signature (222/208 ratio = 1.01). In contrast the linear 6-2-13-5 peptide displays comparatively low helicity (Figure 5b, fH = 18.2%), increasing upon lactamisation to display an improved overall α-helical signature (222/208 = 0.69) but with little change in overall helicity (fH = 20.4%).

Global secondary structure and stability was next monitored by incubating peptides with cJun. At 20°C the linear form of 1-3-16-7 (Figure 6a) showed a helical profile (222/208 = 0.87) with a fractional helicity greater than the average (fH = 55.2%) of the component peptides (ΔfH = 8%). For the lactamised version (Figure 6b), the profile remained highly helical (222/208 = 0.90) with helicity (fH = 52.0%) negligibly greater than the average of the two component peptides (ΔfH = 1.75%). In both the linear and lactamised forms of 6-2-13-5 (Figure 7a,b), levels of helicity were lower. The linear form incubated with cJun displayed no increase in signal (ΔfH = 0.1%) relative to the component peptides. Similarly, the lactamised form showed a level of helicity (fH = 25%) similar to that of the average.

Thermal Denaturation Profiles - Having observed varying levels of helicity between all peptides, CD thermal denaturation experiments were next performed to establish the extent to which the stability of the complexes changed upon introduction of the constraints. In these experiments the 222 nm signal was monitored at 1°C increments from 0°C to 90°C. For linear 1-3-16-7 in isolation (Figure 5C), an interaction was observed (T_m = 29.1°C), which upon lactamisation led to an increase in thermal stability (T_m = 67.0°C). Moreover, the signal persisted even at high temperatures, implying that the lactamised form retains residual thermal stability relative to the linear form. When in complex with cJun (Figure 6C,D), the linear peptide exhibited an increase in T_m (34°C), with the lactamised form displaying a marked increase in thermal stability over the average of the component peptides, demonstrating that the lactamised form of the peptide is able to preferentially bind cJun. The ΔT_m (1-3-16-7_{LAC}:cJun — 1-3-16-7_{LIN}:cJun) was found to be 23°C, demonstrating that dual lactamisation is tolerated and translates into increase target affinity.

For 6-2-13-15, both peptides displayed lower levels of stability (Figure 7C,D), with T_m values unable to be derived from the thermal melt profiles. Consistent with CD spectra, this implies a much lower level of thermal stability in isolation. However, upon incubation with cJun, the linear form displays higher levels of heterodimeric thermal stability (T_m = 18.9°C), which is increased upon lactamisation (T_m = 29.2°C). The ΔT_m (6-2-13-5_{LAC}:cJun — 6-2-13-5_{LIN}:cJun) was found to be 10°C. Overall this suggests that, as reflected in the lower levels of helicity relative to 1-3-16-7_{LAC}:cJun (fH =

25 % vs 52%), the constraint is less well tolerated. Moreover, this consequently translates into a lower overall improvement in target affinity relative to the linear counterpart. Figure 8 highlights the relevance of these modular designs in the wider scheme of engineered peptides that can tolerate constraints and that lead to a demonstrable increase in target affinity for a defined coiled coil target. As previously discussed[22], there are indirect parallels which can be drawn based on T_m. Previous isothermal calorimetry work characterising the biophysical properties of peptides demonstrated a FosW-cJun interaction K_D value of 39 nM[29],which displayed a thermal stability similar to that of the lactamised 1-3-16-7 (T_m = 63°C). Similarly, the 1-3-16-7$_{LAC}$:cJun complex reported the same helicity (fH = 52%) and a similar T_m and K_D to that of cFos-24 (Tm = 58°C; K_D of 7.25 μM)[30]. The comparative values provide a broad understanding of enhanced structural stability displayed in lactamised complexes and demonstrate the potential impact lactamisation may have on biophysical properties, and the ability to predict such properties based upon modular design and experimental validation.

Helix Nucleation **-** The folding of the α-helix is due in large part to the stabilisation conferred by sequential i-i+4 hydrogen bonds. Moreover, α-helices display an overall dipole moment with a pair of terminal micro-dipoles due to a lack of intrahelical hydrogen bonds at the termini. In particular, unsatisfied hydrogen bonding by the first four >N-H groups at the N-terminus can lead to a partial positive charge (δ+). Similarly the last four >C=O groups at the C-terminus can lead to a partial negative charge (δ-)[31]. Instead, these groups are often capped by alternative hydrogen bond partners that are provided by helix-capping motifs[32]. It is therefore generally accepted that charge-macrodipole interactions can play a small role in enhancing the stability of a helix – with negatively charged residues at the N-terminus and positively charged residues at the C-terminus that can counter the effects of the dipole. As highlighted in Figure 4, the designs of our full length α-helix could be optimised to counter the dipole. For peptide 1-3-16-7 Glu was introduced at the N-terminus and Lys at the C-Terminus. However, the control peptide (6-2-13-5) did not provide charge complementarity for the helix macrodipole, containing a Lys at the N-terminus and Glu at the C-terminus. The former peptide is more stable than the latter (either as a homomer or in complex with cJun). Coupled with constraints that are less well tolerated in individual cassettes for the control sequence (average helicity of component cassettes = 57% vs 38%), this suggests that charge stabilisation at both termini, even with addition of less-well tolerated constraints, could be another influencing factor. Coupling the structural stability lactam bridges confer with favourable terminal residues may therefore represent another way to introduce additional target-affinity into the peptide.

Sequence specific Helicities – Due to the limited randomisation and size of the cassette library, there exists an opportunity to further study the effects of the different sequence combinations from the

perspective of helical stability. Despite focusing on peptides longer than 10 residues, the idea of sequence specific stability (in the context of positions ***g/e***) has been discussed previously[20]. The presence of N-terminal Glu and C-terminal Lys might have been expected to lead to the highest helicity values with every different core option. As is shown in Figure 9, there does appear to be a pattern within the library. For each of the 4 core options, it would be expected that the Glu/Lys selection (with a positively charged C-terminus) would yield stability similar to that of the peptide 1-3-16-7. This is partially correct as, regardless of the core arrangement, the E/K cassettes display the highest (Ile/Val) or second highest (Leu/Asn) helicities. When observing the Ile/Leu/Val library members, this electrostatic arrangement resulted in cassettes with helicities 10-23% higher than the next most stable. In the case of Asn, the helicity values are far more similar, with a difference of 10% between the four. In this case the polarity of the core Asn appears likely to be influencing the effect that these terminal charged residues usually impart upon the macrodipole and therefore upon helicity. When considering the inverse, the lowest helicity cassettes are those with Lys at the N-terminus and Glu at the C-terminus. This is logical when considering the arguments proposed previously regarding the helix macrodipole within the 29-mer.

CONCLUSION

We have demonstrated that modular ***gabcdef*** heptad cassettes can be lactamised via sidechain to sidechain K→D (i→i+4) bridges as a mechanism to impart high helicity upon otherwise unstructured sequences. We have shown that although all of the sequences adopt helical conformations, the fractional helicity observed varies in magnitude from 34 to 68% across the 16 lactamised cassettes. It was therefore possible to use the cassettes to create a library that can be conjugated into 4 repeats (16^4 = 65,536 possible combinations) towards creating coiled coil antagonists. Furthermore, we utilised the bCIPA library screening algorithm (http://people.bath.ac.uk/jm2219/biology/iscan.zip) as a means to select peptides that ***i)*** best engage with a heptad counterpart within a target helix and ***ii)*** have a low tendency to self-associate.

Conjugating individual cassettes of high measured helicity (1, 3, 16, 7 = 45%, 60%, 55%, 68% respectively) into a longer sequence constrained by terminal lactams was shown to impart further helicity (fH = 65% linear vs. 71% lactamised), which consequently translated into an increased T_m with the cJun target (34°C linear vs 57°C lactamised). In contrast, a control sequence in which component cassettes were known to lactamised comparatively poorly (6, 2, 13, 5 = 36%, 34%, 47 %, 41%), was lactamised at the termini with only a negligible gain in helicity observed (fH = 18% linear vs. 20% lactamised), which translated into only a modest gain in T_m with the cJun target (19°C linear vs 29°C lactamised).

Since all cassettes exhibited increased helicity when lactamised, this poses an interesting question regarding the ability of certain sequences to adopt a more helical conformation than others (Figure 3, Figure 9). Since the possible permutations within the 16 peptides were limited, there a limit to the information that can be drawn in terms of electrostatic and core configuration that optimise the stability of the cassettes. However, the placement of Glu at the N-terminal ***g*** position appears to impart increased helicity over all other options unless Asn resides at the core ***a*** position. The placement of Lys at the C-terminal ***e*** position appears to be less influential on its own but does complement the placement of an N-terminal Glu at the ***g*** position. Placement of Lys at the ***g*** position and Glu at the ***e*** position results in the lowest helical values of all cassettes but is tempered slightly by the placement of Asn at the ***a*** position. With more data, this presents an opportunity to optimise computational techniques employed for prediction. As previously shown,[22] bCIPA is capable of being trained on a specific subset of coiled coil forming sequences. With further experimental exploration of the cassette library, reflecting other cassette types observed within natural coiled coils, it will be possible to extract more helical predictors towards developing a more robust prediction algorithm that can specifically consider lactamised peptides. For instance, further interrogation of the system could involve expanding the cassette library to include residues with larger side-chains, or side-chains which have been previously shown to be non-optimal at certain sequence positions in the design of α-helical peptides. In this study we have probed the ability of given coiled coil sequences to tolerate the introduction of K→D lactam bridges between solvent exposed ***b*** and ***f*** residues. Once established that lactams are tolerated then the precise level of helical induction can be calculated. However, the assumption that molecules with increasingly higher helicity might better form coiled coils, is an oversimplification[29,30,33]. Rather, there is likely a limit to the entropy value of preorganizing a helical structure. Above a certain threshold helicity, conformational entropy may serve to oppose coiled-coil formation[34], perhaps reflecting the need for some residual helix flexibility to enable the distortion necessary for supercoiling[35,36].

The properties of cassettes with high levels of stability in comparison to others will allow further understanding of the rules by which b→f lactamisation imparts helicity. As further experimental data is acquired, computational techniques employed in the selection of cassettes for specific functions will be refined. These “off-the-shelf” sequences can be combined with computational screening and applied to a wide range of parallel dimeric coiled coil dimerization domains as a generalised method to ablate or even agonise the function of a wide range of proteins in which parallel and dimeric coiled coils are found.

MATERIALS AND METHODS

bCIPA Peptide Library Screening - bCIPA screening was performed as described previously[22]. Briefly, individual sequences of cassettes were calculated as homodimers and with the cJun target sequence using software based on the bCIPA algorithm[28]. Thermal denaturation (T_m) values were normalised. Peptide Synthesis - Rink amide ChemMatrix™ resin was obtained from PCAS Biomatrix, Inc. (St.-Jean-sur-Richelieu, Canada); Fmoc L-amino acids and 2-(1H-benzotriazole-1-yl)-1,1,3,3-tetra-methyluronium hexafluorophosphate (HBTU) or benzotriazol-1-yl-ox-ytripyrrolidinophosphonium hexafluorophosphate (PyBOP) were obtained from AGTC Bioproducts (Hessle, UK); all other reagents were of peptide synthesis grade and obtained from ThermoFisherScientific (Loughborough,UK). Peptides were synthesised on a 0.1-mmol scale on a PCAS ChemMatrix™ Rink amide resin using a Liberty Blue™ microwave peptide synthesiser (CEM; Matthews, NC) employing Fmoc solid-phase techniques[37] with repeated steps of coupling, deprotection and washing (4 × 5 ml dimethylformamide). Coupling was performed as follows: Fmoc amino acid (5 eq), HBTU or PyBOP (4.5 eq) and diisopropylethylamine (10 eq) in dimethylformamide (5 ml) for 5 min with 35-W microwave irradiation at 90 °C. Deprotection was performed as follows: 20% piperidine in dimethylformamide for 5 min with 30-W microwave irradiation at 80 °C. Following synthesis, peptides were acetylated using acetic anhydride (3 eq) and diisopropylethylamine (4.5 eq) in dimethylformamide(2.63 ml) for 20 min. Deprotection of acid labile Asp(oPip) and Lys(Mtt) side chain protecting groups was achieved by repeated washing of the resin in dichloromethane, followed by repeated washes in dichloromenthane (2% TFA), dichloromethane, and finally dimethylformamide. Resin was next incubated for 7 hours at 55°C in 2-(1H-benzotriazole-1-yl)-1,1,3,3 tetramethyluronium hexafluorophosphate (1ml), diisopropylethylamine (1ml), and dimethylformamide (3ml). Resin was filtered and cleaved from the resin with concomitant removal of side-chain-protecting groups by treatment with a cleavage mixture (10 ml) consisting of TFA (95%), triisopropylsilane (2.5%) and H_2O (2.5%) for 4 h at room temperature. Suspended resin was removed by filtration, and the peptide was precipitated using three rounds of crashing in ice-cold diethyl ether, vortexing and centrifuging. The pellet was then dissolved in 1:1MeCN/H_2O and freeze-dried. Purification was performed by RP-HPLC using a Phenomenex Jupiter Proteo (C18) reverse-phase column (4 µm, 90 Å, 10 mm inner diameter × 250 mm long). Eluents used were as follows: 0.1% TFA in H_2O (a) and 0.1% TFA in ACN (b). The peptide was eluted by applying a linear gradient (at 3.5 ml/min) of 5–95% B over 50 min. Fractions collected were examined by electrospray MS, and those found to contain exclusively the desired product were pooled and lyophilised. Analysis of the purified final product by RP-HPLC indicated a purity of >95%.

Peptide Quantification – Peptide concentrations were determined in dd$H_2$0 or CD buffer (10 mM potassium phosphate and 100 mM potassium fluoride, pH 7) against the appropriate blank using the

280 nm absorbance maxima of the Tyr residue within each peptide (1209 $M^{-1}cm^{-1}$). Prior to each measurement samples were centrifuged at 13,000 rpm for 2 minutes to ensure that only soluble peptide was quantified. During this step no precipitate was observed, indicating that all peptides displayed high levels of solubility. Measurements were taken using a Varian Cary 50 Conc UV Spectrophotometer using a 1 cm pathlength quartz cell.

Circular Dichroism - CD was carried out using an Applied Photophysics Chirascan CD apparatus (Leatherhead, UK) using a 200-µl sample in a CD cell with a 1-mm path length. Samples contained 150 µM total peptide (Pt) concentration at equimolar concentration for heterodimeric solutions (i.e., 75 µM per peptide) and suspended in 10 mM potassium phosphate and 100 mM potassium fluoride at pH 7 for 30 minutes prior to analysis. The CD spectra of samples were scanned between 300 nm and 190 nm in 1 nm steps, averaging 0.5 s at each wavelength. Three scans at 20 °C were averaged to assess helical levels and CC structure. For thermal scans, spectra were scanned as above in 10°C steps from 20°C to 90°C. Each temperature point was held for 1 min to equilibrate sample before scanning. Raw data (ellipticities) were collected and averaged, and data were converted to molar residue ellipticities (MRE).

All spectral data was converted to fractional helicity (fH) values according to the equation:

$$fH = \frac{\Theta_{222} - \Theta_c}{\Theta_{222\infty} - \Theta_c} \quad (1)$$

$$\Theta_c = 2220 - (53 \times T)$$

$$\Theta_{222\infty} = (-44000 + (250 \times k)) \times (1 - \frac{k}{Nr})$$

Where the wavelength-dependent constant k = 2.4 (at 222nm), Nr = number of residues, and T = temperature (°C).

Thermal Denaturation – Thermal denaturation experiments were performed at 150 µM in a buffer of 10 mM potassium phosphate and 100 mM potassium fluoride at pH 7 using an Applied Photophysics Chirascan Circular Dichroism Spectrometer. For all thermal denaturation experiments involving longer peptides, a stepping gradient was applied from 0°C to 90°C using 1°C increments. Each temperature point was held for 30 seconds to equilibrate the sample before measuring ellipticity at 222 nm. Melting profiles were converted to equilibrium denaturation curves and fitted using a two-state model, derived via modification of the Gibbs–Helmholtz equation to yield the melting temperature (T_m)[28].

AUTHOR CONTRIBUTIONS

AL conducted experiments, and synthesized, purified and characterised peptides and cJun. JMM directed the research. Both authors participated in experimental design, analysis of the data, and writing the paper.

COMPETING FINANTIAL INTERESTS

JMM is an advisor to Sapience Therapeutics. AL has no financial or commercial conflict to declare.

ACKNOWLEDGEMENTS

J.M. and A.L thank the University of Bath for a Studentship. J.M. is also grateful to Cancer Research UK (A11738 and A26941) and to the BBSRC (BB/R017956/1) and EPSRC (EP/M001873/1).

SUPPORTING INFORMATION

Supporting information is available in Supplementary Figures S1-S8 and Supplementary Tables S1-S2 with associated legends online. This material is available free of charge via the internet at http://pubs.acs.org.

REFERENCES

(1) Walensky, L. D., and Bird, G. H. (2015) Hydrocarbon-Stapled Peptides: Principles, Practice, and Progress. *J. Med. Chem. 57*, 6275–6288.

(2) De Araujo, A. D., Hoang, H. N., Kok, W. M., Diness, F., Gupta, P., Hill, T. A., Driver, R. W., Price, D. A., Liras, S., Fairlie, D. P., de Araujo, A. D., Hoang, H. N., Kok, W. M., Diness, F., Gupta, P., Hill, T. A., Driver, R. W., Price, D. A., Liras, S., and Fairlie, D. P. (2014) Comparative α-helicity of cyclic pentapeptides in water. *Angew. Chemie - Int. Ed. 53*, 6965–6969.

(3) Acharyya, A., Ge, Y., Wu, H., DeGrado, W. F., Voelz, V. A., and Gai, F. (2019) Exposing the Nucleation Site in α-Helix Folding: A Joint Experimental and Simulation Study. *J. Phys. Chem. B* acs.jpcb.8b12220.

(4) Hilinski, G. J. (2012) Stapled Peptides for Intracellular Drug Targets. *Methods Enzymol. 503*, 3–33.

(5) Tan, Y. S., Lane, D. P., and Verma, C. S. (2016) Stapled peptide design: principles and roles of computation. *Drug Discov. Today 21*, 1642–1653.

(6) Pal, S., and Prabhakaran, E. N. (2018) Hydrogen bond surrogate stabilized water soluble 310-helix from a disordered pentapeptide containing coded α-amino acids. *Tetrahedron Lett. 59*, 2515–2519.

(7) Patgiri, A., Jochim, A. L., and Arora, P. S. (2008) A Hydrogen Bond Surrogate Approach for Stabilization of Short Peptide Sequences in α-Helical Conformation. *Acc. Chem. Res. 41*, 1289–1300.

(8) Estieu-Gionnet, K., and Guichard, G. (2011) Stabilized helical peptides: overview of the technologies

and therapeutic promises. *Expert Opin. Drug Discov. 6*, 937–963.

(9) Lau, Y. H., De Andrade, P., Wu, Y., and Spring, D. R. (2015) Peptide stapling techniques based on different macrocyclisation chemistries. *Chem. Soc. Rev. 44*, 91–102.

(10) Pelay-Gimeno, M., Glas, A., Koch, O., and Grossmann, T. N. (2015) Structure-Based Design of Inhibitors of Protein-Protein Interactions: Mimicking Peptide Binding Epitopes. *Angew. Chemie - Int. Ed. 54*, 8896–8927.

(11) Shepherd, N. E., Hoang, H. N., Abbenante, G., and Fairlie, D. P. (2005) Single turn peptide alpha helices with exceptional stability in water. *J. Am. Chem. Soc. 127*, 2974–2983.

(12) Shepherd, N. E., Abbenante, G., and Fairlie, D. P. (2004) Consecutive cyclic pentapeptide modules form short alpha-helices that are very stable to water and denaturants. *Angew. Chemie - Int. Ed. 43*, 2687–2690.

(13) Tala, S. R., Schnell, S. M., and Haskell-Luevano, C. (2015) Microwave-assisted solid-phase synthesis of side-chain to side-chain lactam-bridge cyclic peptides. *Bioorganic Med. Chem. Lett. 25*, 5708–5711.

(14) Harrison, R. S., Shepherd, N. E., Hoang, H. N., Ruiz-Gomez, G., Hill, T. A., Driver, R. W., Desai, V. S., Young, P. R., Abbenante, G., and Fairlie, D. P. (2010) Downsizing human, bacterial, and viral proteins to short water-stable alpha helices that maintain biological potency. *Proc. Natl. Acad. Sci. 107*, 11686–11691.

(15) Hoang, H. N., Driver, R. W., Beyer, R. L., Hill, T. A., D. de Araujo, A., Plisson, F., Harrison, R. S., Goedecke, L., Shepherd, N. E., and Fairlie, D. P. (2016) Helix Nucleation by the Smallest Known α-Helix in Water. *Angew. Chemie - Int. Ed. 55*, 8275–8279.

(16) Hoang, H. N., Song, K., Hill, T. A., Derksen, D. R., Edmonds, D. J., Kok, W. M., Limberakis, C., Liras, S., Loria, P. M., Mascitti, V., Mathiowetz, A. M., Mitchell, J. M., Piotrowski, D. W., Price, D. A., Stanton, R. V., Suen, J. Y., Withka, J. M., Griffith, D. A., and Fairlie, D. P. (2015) Short hydrophobic peptides with cyclic constraints are potent glucagon-like peptide-1 receptor (GLP-1R) agonists. *J. Med. Chem. 58*, 4080–4085.

(17) Seebach, D., and Fadel, A. (1985) N,O-Acetals from Pivalaldehyde and Amino Acids for the ?-Alkylation with Self-Reproduction of the Center of Chirality. Enolates of 3-Benzoyl-2-(tert-butyl)-1,3-oxazolidin-5-ones. *Helv. Chim. Acta 68*, 1243–1250.

(18) Mason, J. M., Schmitz, M. A., Muller, K. M., and Arndt, K. M. (2006) Semirational design of Jun-Fos coiled coils with increased affinity: Universal implications for leucine zipper prediction and design. *Proc. Natl. Acad. Sci. 103*, 8989–8994.

(19) Hagemann, U. B., Mason, J. M., Müller, K. M., and Arndt, K. M. (2008) Selectional and Mutational Scope of Peptides Sequestering the Jun-Fos Coiled-Coil Domain. *J. Mol. Biol. 381*, 73–88.

(20) Crooks, R. O., Baxter, D., Panek, A. S., Lubben, A. T., and Mason, J. M. (2016) Deriving Heterospecific Self-Assembling Protein-Protein Interactions Using a Computational Interactome

Screen. *J. Mol. Biol. 428*, 385–398.

(21) Crooks, R. O., Lathbridge, A., Panek, A. S., and Mason, J. M. (2017) Computational Prediction and Design for Creating Iteratively Larger Heterospecific Coiled Coil Sets. *Biochemistry 56*, 1573–1584.

(22) Lathbridge, A., and Mason, J. M. (2018) Computational Competitive and Negative Design to Derive a Specific cJun Antagonist. *Biochemistry 57*, 6108–6118.

(23) Hill, T. A., Shepherd, N. E., Diness, F., and Fairlie, D. P. (2014) Constraining cyclic peptides to mimic protein structure motifs. *Angew. Chemie - Int. Ed. 53*, 13020–13041.

(24) Mason, J. M., Müller, K. M., and Arndt, K. M. (2007) Positive aspects of negative design: Simultaneous selection of specificity and interaction stability. *Biochemistry 46*, 4804–4814.

(25) Mason, J. M., Müller, K. M., and Arndt, K. M. (2007) Considerations in the design and optimization of coiled coil structures., in *Methods in molecular biology (Clifton, N.J.)*, pp 35–70. Springer.

(26) Mason, J. M., and Arndt, K. M. (2004) Coiled coil domains: Stability, specificity, and biological implications. *ChemBioChem 5*, 170–176.

(27) Fletcher, J. M., Bartlett, G. J., Boyle, A. L., Danon, J. J., Rush, L. E., Lupas, A. N., and Woolfson, D. N. (2017) N@ a and N@ d: Oligomer and Partner Specification by Asparagine in Coiled-Coil Interfaces. *ACS Chem. Biol. 12*, 528–538.

(28) Mason, J. M., Hagemann, U. B., and Arndt, K. M. (2007) Improved stability of the Jun-Fos activator protein-1 coiled coil motif: A stopped-flow circular dichroism kinetic analysis. *J. Biol. Chem. 282*, 23015–23024.

(29) Baxter, D., Perry, S. R., Hill, T. A., Kok, W. M., Zaccai, N. R., Brady, R. L., Fairlie, D. P., and Mason, J. M. (2017) Downsizing Proto-oncogene cFos to Short Helix-Constrained Peptides That Bind Jun. *ACS Chem. Biol. 12*, 2051–2061.

(30) Rao, T., Ruiz-Gómez, G., Hill, T. A., Hoang, H. N., Fairlie, D. P., and Mason, J. M. (2013) Truncated and Helix-Constrained Peptides with High Affinity and Specificity for the cFos Coiled-Coil of AP-1. *PLoS One* (Sanchez-Ruiz, J. M., Ed.) *8*, e59415.

(31) Ganesan, S. J., and Matysiak, S. (2014) Role of Backbone Dipole Interactions in the Formation of Secondary and Supersecondary Structures of Proteins.

(32) Aurora, R., and Rosee, G. D. (1998) Helix capping. *Protein Sci. 7*, 21–38.

(33) Dragan, A. I., and Privalov, P. L. (2002) Unfolding of a Leucine zipper is not a Simple Two-state Transition. *J. Mol. Biol. 321*, 891–908.

(34) Worrall, J. A. R., and Mason, J. M. (2011) Thermodynamic analysis of Jun-Fos coiled coil peptide antagonists. *FEBS J. 278*, 663–672.

(35) Crick, F. H. C. (1953) The packing of α-helices: simple coiled-coils. *Acta Crystallogr.*, pp 689–697. International Union of Crystallography (IUCr).

(36) Pauling, L., Corey, R. B., and Branson, H. R. (1951) The structure of proteins; two hydrogen-bonded

helical configurations of the polypeptide chain. *Proc. Natl. Acad. Sci. U. S. A. 37*, 205–11.
(37) Fields, G. B., and Noble, R. L. (1990) Solid phase peptide synthesis utilizing 9-fluorenylmethoxycarbonyl amino acids. *Int. J. Pept. Protein Res. 35*, 161–214.

Figure Legends:

Figure 1. Design of heptad cassette sequences. Peptide options are randomised around electrostatic positions g and e (Glu/Lys) and core position a (Ile/Leu/Val/Asn). This illustrates the diverse options available at the hydrophobic interface and the different charge profiles available for electrostatic interactions. The lactam bridge between b-f (Lys-to-Asp) is also shown.

Figure 2. CD spectra for cassettes 1-16. These are shown in both the linear (black) and lactamised (red) forms. Spectra were measured at 20 °C at a total peptide concentration of 150 μM and presented as mean residue ellipticity (MRE). All experiments were performed in 10 mM potassium phosphate and 100 mM potassium fluoride (pH 7). In all cases, the linear forms were characterised as having a random coil profile – with an average 222 nm/208 nm ratio of 0.24. The lactamised cassettes displayed more of a helical profile – with an average ratio of the signal at 222 nm/208 nm of 0.79.

Figure 3. Fractional helicity (fH) data for Cassettes 1-16. (A) shows values calculated from the 222 nm value from circular dichroism scans at 20°C. For each cassette, the cyclic (lactamised) form has increased helicity compared to the linear (black), with an average increase of 37.6%. The ΔfH values (B) show that the largest increase in helicity was seen in Cassette 16 (ΔfH = 50.63%) whereas the lowest increase in helicity was seen in Cassette 8 (ΔfH = 22.57%). Highlighted are the cassettes used in the full-length peptide (*) and those used in the control (+).

Figure 4. Design of lactamised sequences. Shown are 1-3-16-7 (A) and control 6-2-13-5 (B). In both cases cassettes were chosen independently of one another. For 1-3-16-7, considering the cassettes in isolation, there is a mixture of electrostatically repulsive (cassette 1), favourable (cassette 3), and non-optimal (cassette 16). For heptad 3 (C), the Asn-Asn interaction has been selected for at the core. For 6-2-13-5 there is a mixture of electrostatically favourable (cassette 6), partially favourable (cassettes 2,5), and non-optimal (cassette 13). For heptad 3 (C), the Asn-Asn interaction has been selected for at the core. C: Sequences for peptides 1-3-16-7 and 6-2-13-5. The addition of a Tyr at the N-terminus creates a 29 residue peptide that starts at the f position and ends at the f position. Highlighted in green are the cassettes which have Lys/Asp lactamisation (1 and 7 / 6 and 5).

Figure 5. CD spectra and thermal denaturation data for linear and lactamised peptides in isolation. Shown are data for 1-3-16-7 (A and C) and 6-2-13-5 (B and D). Spectra were measured at 20 °C at a total peptide concentration of 150 μM and presented as mean residue ellipticity (MRE). The minima at 208 and 222 nm are indicative of a helical structure, with the 222 nm/208 nm ratio of the lactamised 1-3-16-7 showing more structure (222 nm/208 nm = 1.01) than the linear (222 nm/208 nm = 0.89). The lactamised 6-2-13-5 shows increased helical structure (222 nm/208 nm =0.69) compared to the linear (222 nm/208 nm =0.44) This suggests that the addition of lactam bridges improves the α-helicity in both peptides. Thermal denaturation profiles of linear and lactamised 1-3-16-7 (C) and 6-2-13-5(D) peptides were taken using 1°C increments and tracking the 222 nm signal at 150 μM. Lactamised 1-3-16-7 shows an increase in the transition midpoint with a T_m of 67.0°C compared to the linear T_m of 29.1°C. Lactamised 6-2-13-5 demonstrates a change* in the transition midpoint when in complex with cJun compared to the linear*. All experiments were performed in 10 mM potassium phosphate and 100 mM potassium fluoride (pH 7). Where possible (C), data were fitted to the two-state model.

Figure 6. CD spectra and thermal denaturation data for linear and lactamised 1-3-16-7 with cJun. Shown are data for 1-3-16-7 peptide in the linear (A and C) and lactamised (B and D) in complex with cJun. Spectra were measured at 20 °C at a total peptide concentration of 150 μM and presented as mean residue ellipticity (MRE). The minima at 208 and 222 nm are indicative of a helical structure, with the 222 nm/208 nm ratio of the linear peptide with cJun showing similar structure (222 nm/208 nm = 0.87) to the homomeric complex (222 nm/208 nm = 0.89). The lactamised form displays a decreased helical structure (222 nm/208 nm =0.90) compared to homomeric state (222 nm/208 nm =1.01). Thermal denaturation profiles of homomeric 1-3-16-7 and in complex with cJun (C and D) were measured using 1°C increments and tracking the 222 nm signal at 150 μM. Linear 1-3-16-7 displays an increase in the transition midpoint when in complex with cJun (C), with a T_m of 34°C compared to the homomer (Tm = 29.1°C). Lactamised 1-3-16-7 demonstrates a decrease in the transition midpoint, with a T_m value of 57.2°C when in complex with cJun compared to the homomer Tm of 67°C (cJun T_m = 25.8°C). All experiments were performed in 10 mM potassium phosphate and 100 mM potassium fluoride (pH 7). Where possible (D), data were fitted to the two-state model.

Figure 7. CD spectra and thermal denaturation data for linear and lactamsied 6-2-13-5 with cJun. Shown are data for 6-2-13-5 peptide in the linear (A and C) and lactamised (B and D) in complex with cJun. Spectra were measured at 20 °C at a total peptide concentration of 150 μM and presented as mean residue ellipticity (MRE). The minima at 208 and 222 nm are indicative of various levels of helical structure, with the 222 nm/208 nm ratio of the linear peptide with cJun showing increased structure (222 nm/208 nm = 0.60) to the homomeric complex (222 nm/208 nm = 0.44). The lactamised form

shows increased structure (222 nm/208 nm =0.74) compared to homomeric state (222 nm/208 nm =0.69). This implies that the addition of cJun increased the helicity of the lactamised and linear peptide. Thermal denaturation profiles of homomeric 6-2-13-5 and in complex with cJun (C and D) were taken using 1°C increments and tracking the 222 nm signal at 150 μM. Linear 6-2-13-5 shows an increase in the transition midpoint when in complex with cJun (C), demonstrating a Tm of 18.9°C compared to the homomer*. Lactamised 6-2-13-5 demonstrates an in the transition midpoint, with a Tm value of 25.0°C when in complex with cJun compared to the homomer*. All experiments were performed in 10 mM potassium phosphate and 100 mM potassium fluoride (pH 7). Where possible (D), data were fitted to the two-state model . *Denaturation profiles for homomeric 6-2-13-5 (linear and lactamised) were unable to be fit.

Figure 8. A comparison of the full-length peptides. The T_m of lactamised 1-3-16-7 was 71.4°C as a homomer and 57.2°C in complex with cJun. x indicates an inability to determine a T_m from the melt profile and represents a low stability complex.

Figure 9. Analysis of individual cassette composition demonstrates stability to be sequence specific. Across the library, a Lys/Glu combination at positions g/e result in decreased helicity. Conversely, the selection of Glu/Lys at these positions results in higher levels of helicity – with a delta of 10-23% between cassettes 7/9/11 and the next most stable cassettes. Asn containing cassettes exhibited similar patterns, although the differences between helicity values within the 4 cassettes was shown to be minimal (a delta of 10% within C13-16).

Table 1. The Comparative Helicity of Cassettes 1-16. Sequences for Cassettes 1-16 are shown with linear and cyclic fH values (and the difference) as determined by circular dichroism at 20°C. Cassettes with the highest (red) and lowest (blue) cyclic fH values are highlighted.

Table 2. Selection of Cassettes For Conjugation. Heptads 1-4 of cJun (shown in red) have been predicted against each of the cassettes, alongside the helicity of the lactamised forms from circular dichroism. The bCIPA heterodimer values (cassette – cJun) have been normalised to account for all values <0. Highlighted in green are the cassettes chosen for the full-length alpha helix. Highlighted in yellow are the cassettes chosen for the full-length control peptide, chosen by the predicted T_m alone. For heptad 3, the only cassettes considered were 13-16 (since they contain Asn at the ***a*** position). Cassettes were chosen sequentially, and no cassette was selected multiple times. In total 16^4 cassette combinations were possible leading to 65,536 potential peptide sequences.

Figure 1

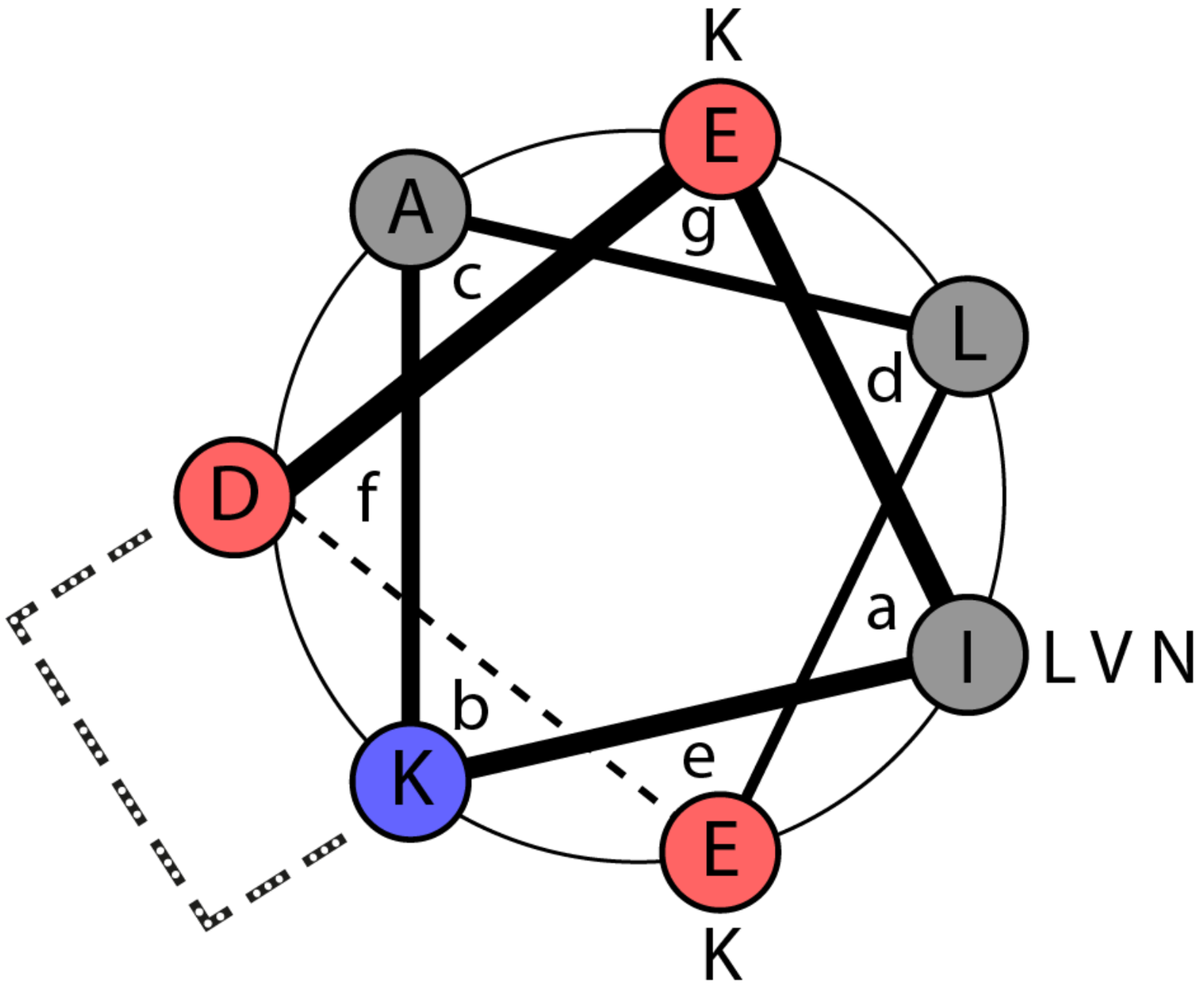

Figure 2

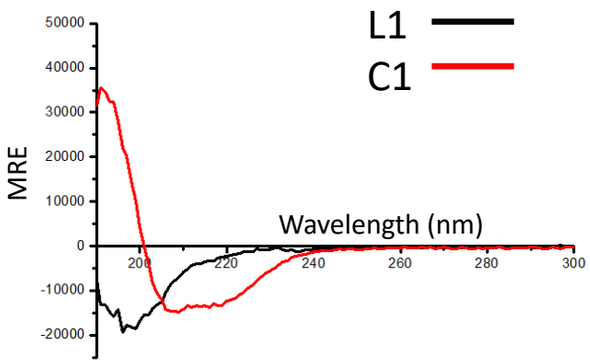
L1
C1
MRE
Wavelength (nm)

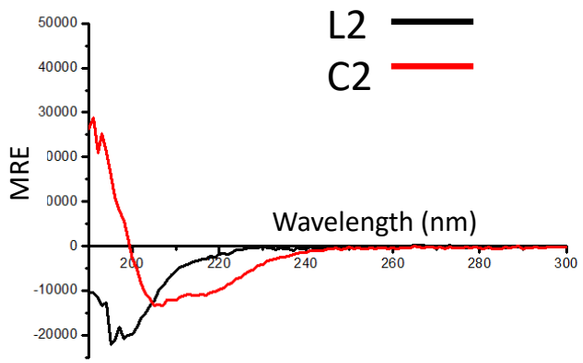
L2
C2
MRE
Wavelength (nm)

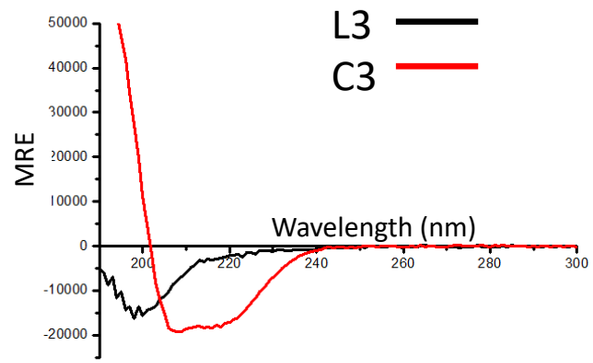
L3
C3
MRE
Wavelength (nm)

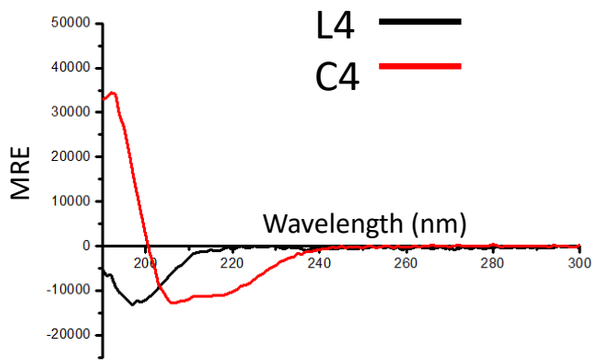
L4
C4
MRE
Wavelength (nm)

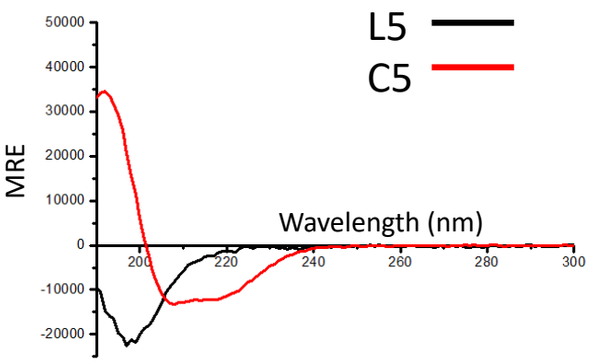
L5
C5
MRE
Wavelength (nm)

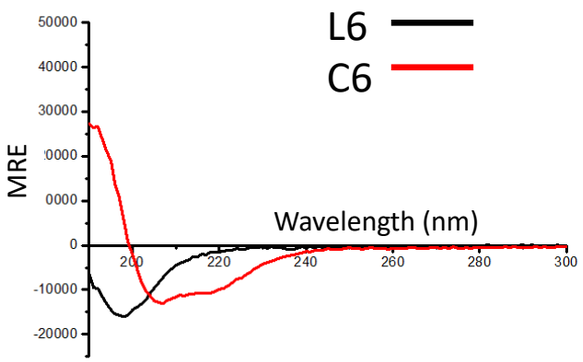
L6
C6
MRE
Wavelength (nm)

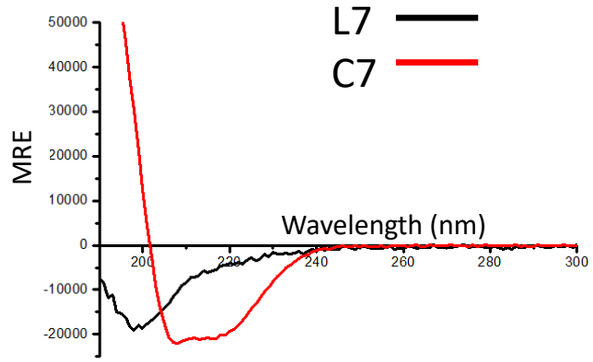
L7
C7
MRE
Wavelength (nm)

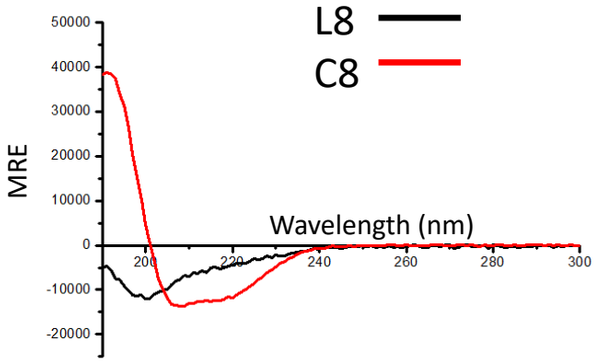
L8
C8
MRE
Wavelength (nm)

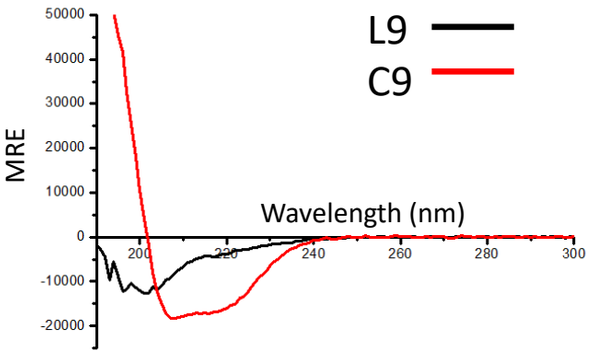
L9
C9
MRE
Wavelength (nm)

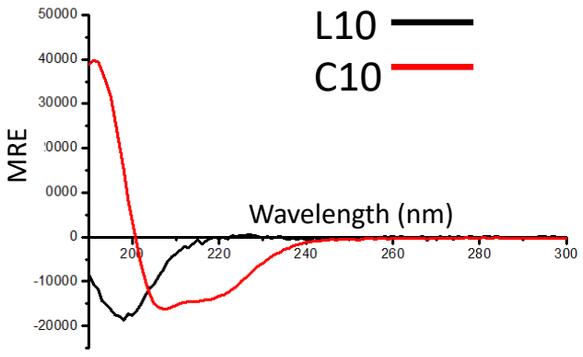
L10
C10
MRE
Wavelength (nm)

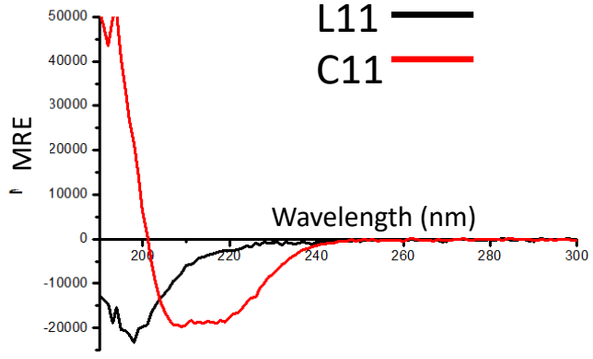
L11
C11
MRE
Wavelength (nm)

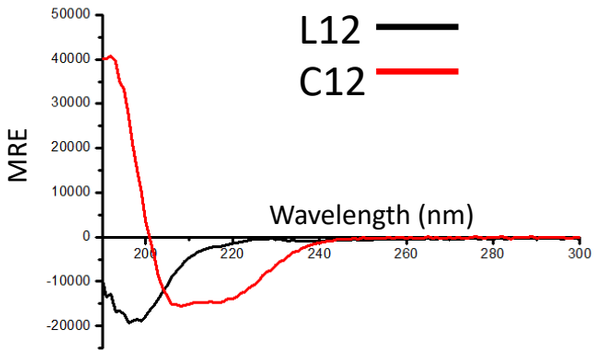
L12
C12
MRE
Wavelength (nm)

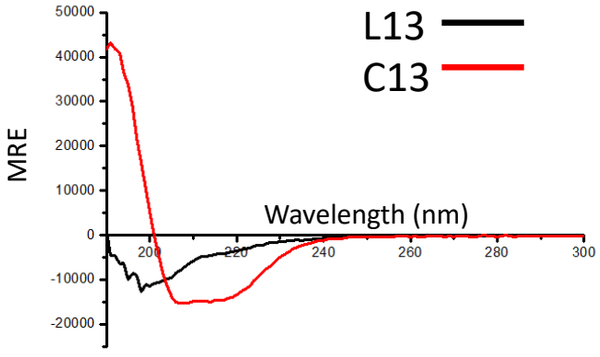
L13
C13
MRE
Wavelength (nm)

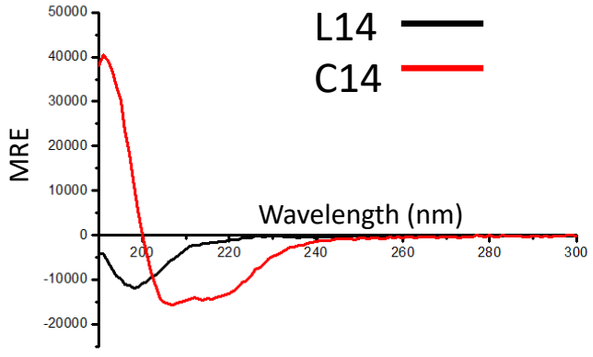
L14
C14
MRE
Wavelength (nm)

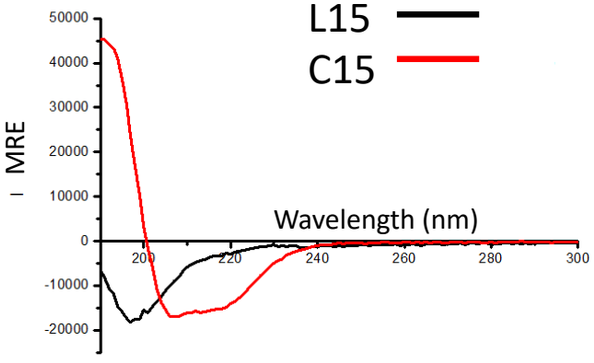
L15
C15
MRE
Wavelength (nm)

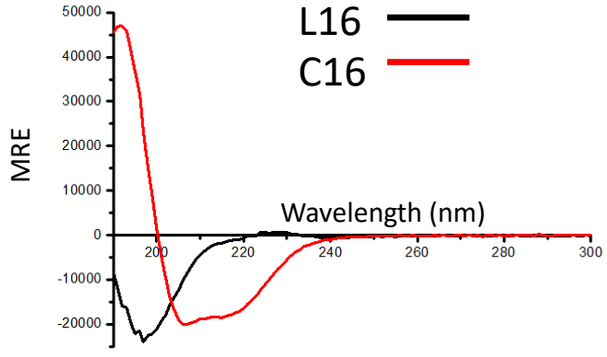
L16
C16
MRE
Wavelength (nm)

Figure 3

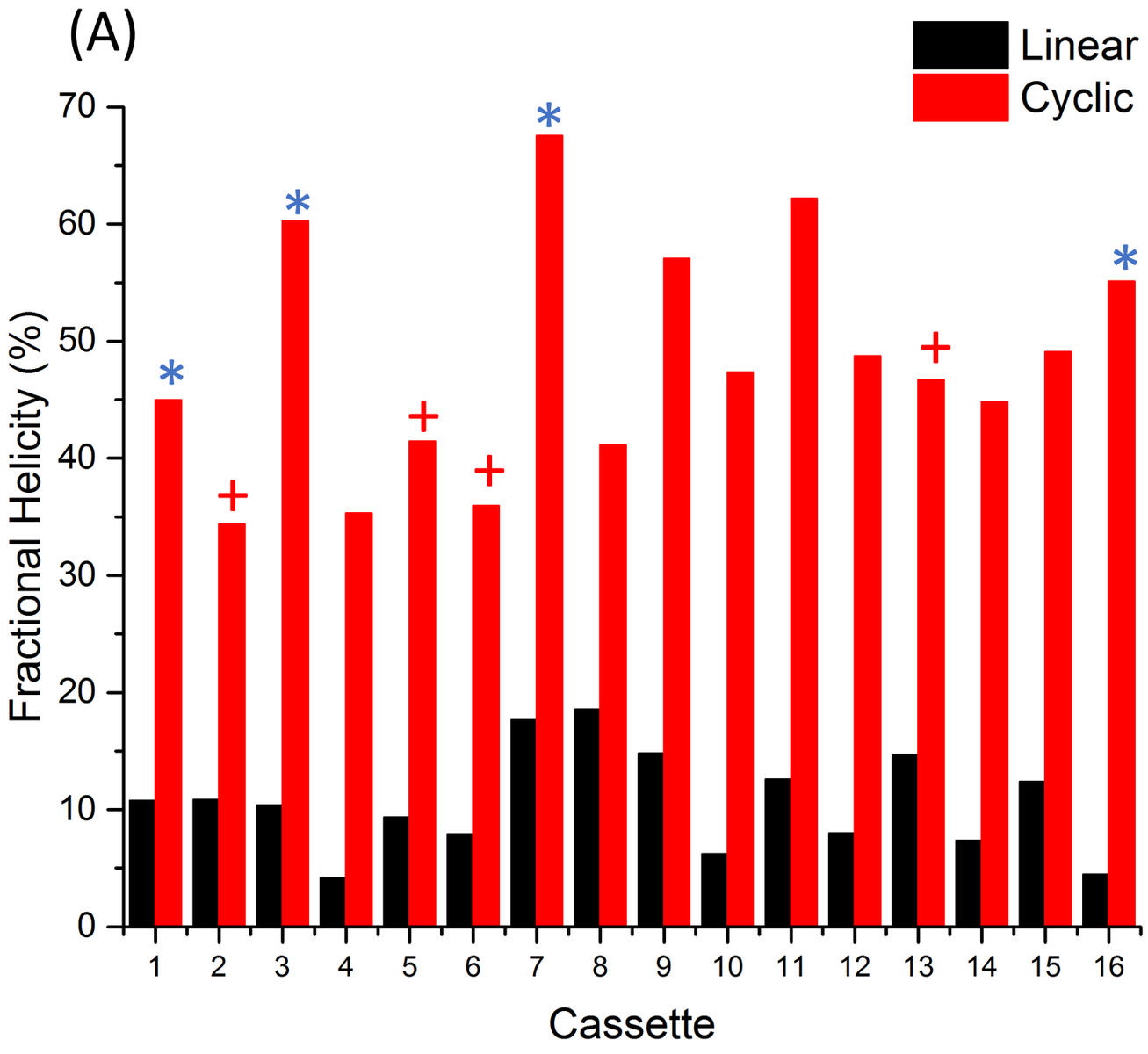
(A)
Linear
Cyclic
Fractional Helicity (%)
0
10
20
30
40
50
60
70
1
2
3
4
5
6
7
8
9
10
11
12
13
14
15
16
Cassette

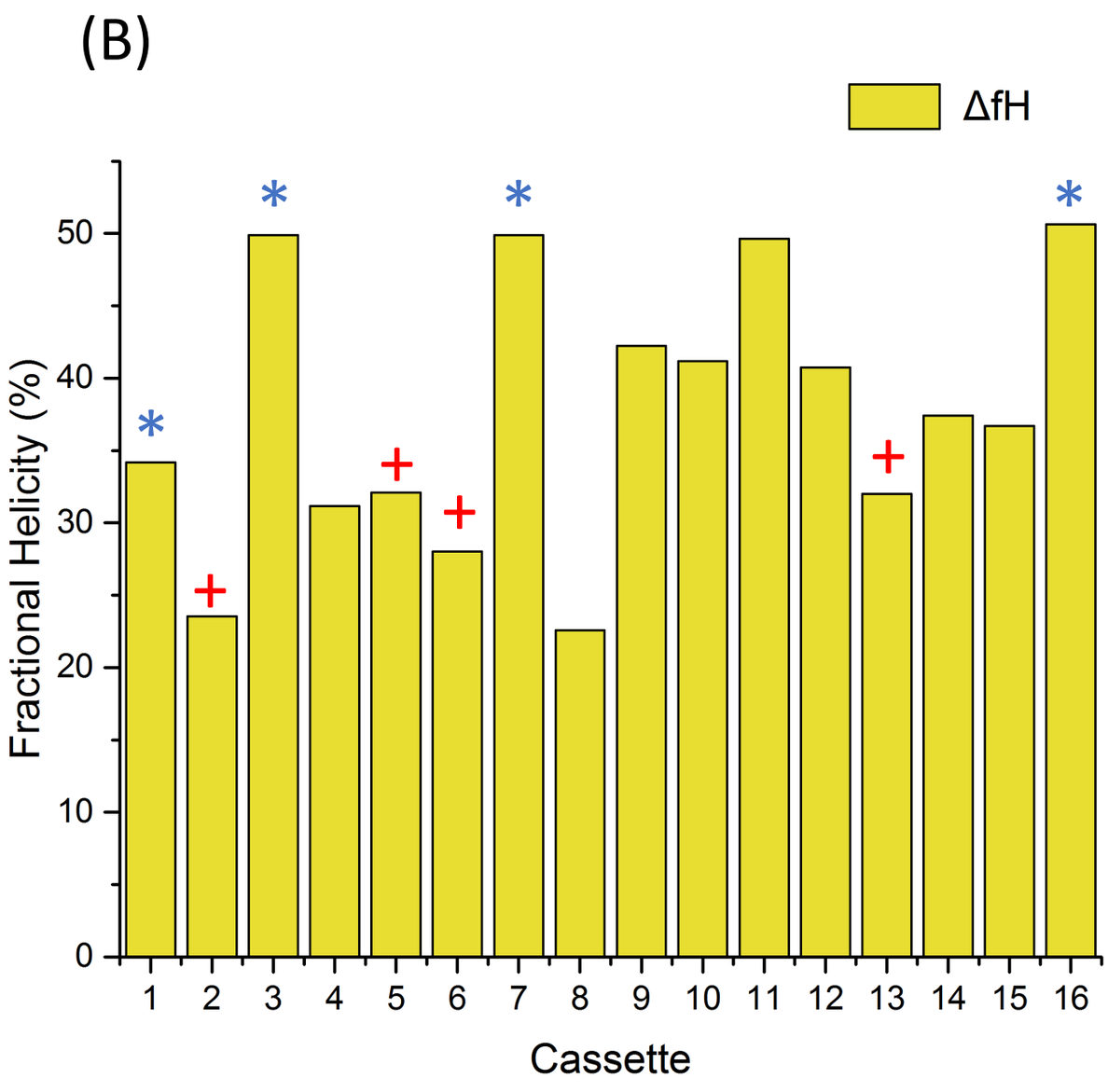
(B)
ΔfH
Fractional Helicity (%)
0
10
20
30
40
50
1
2
3
4
5
6
7
8
9
10
11
12
13
14
15
16
Cassette

Figure 4

(A)

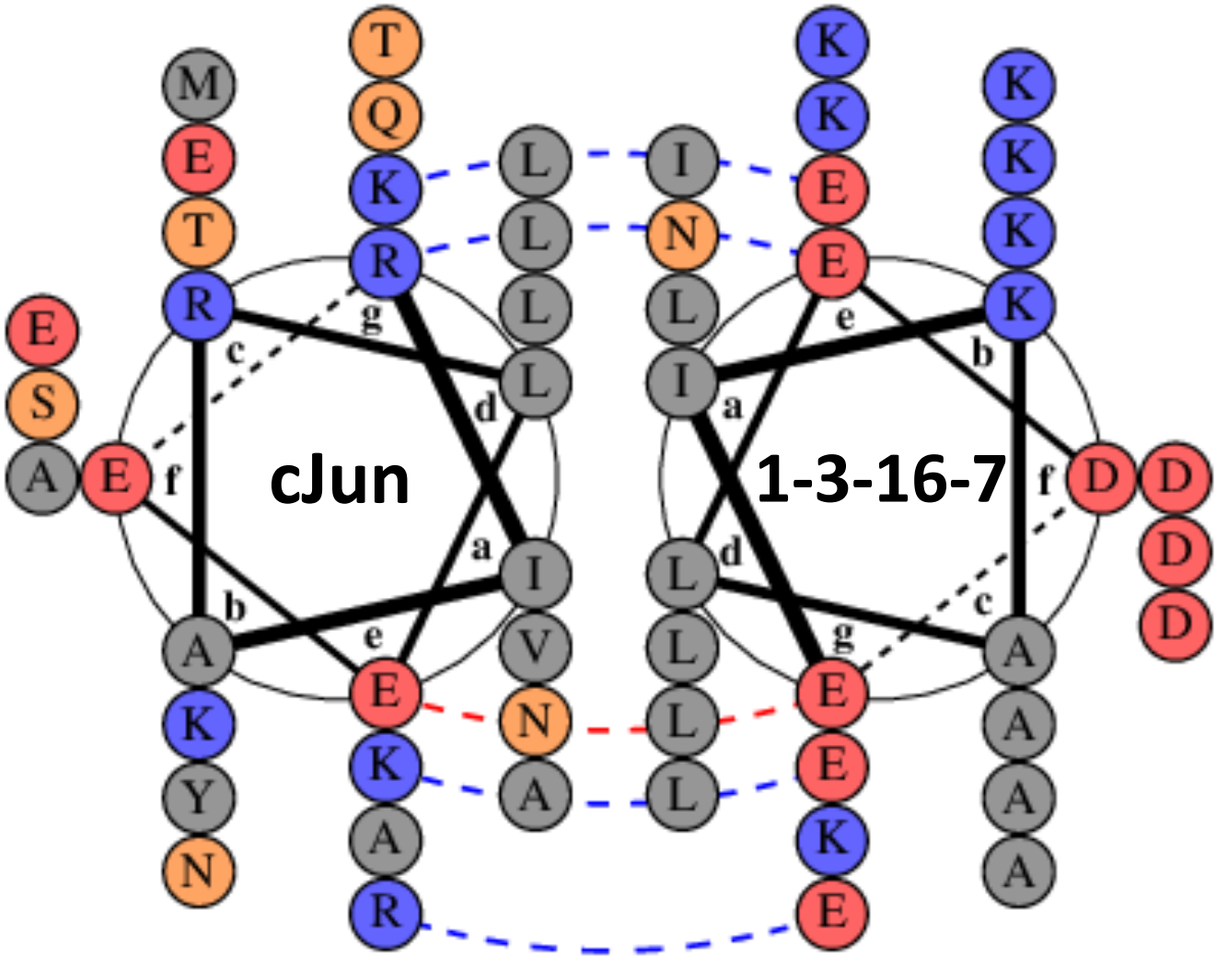

(B)

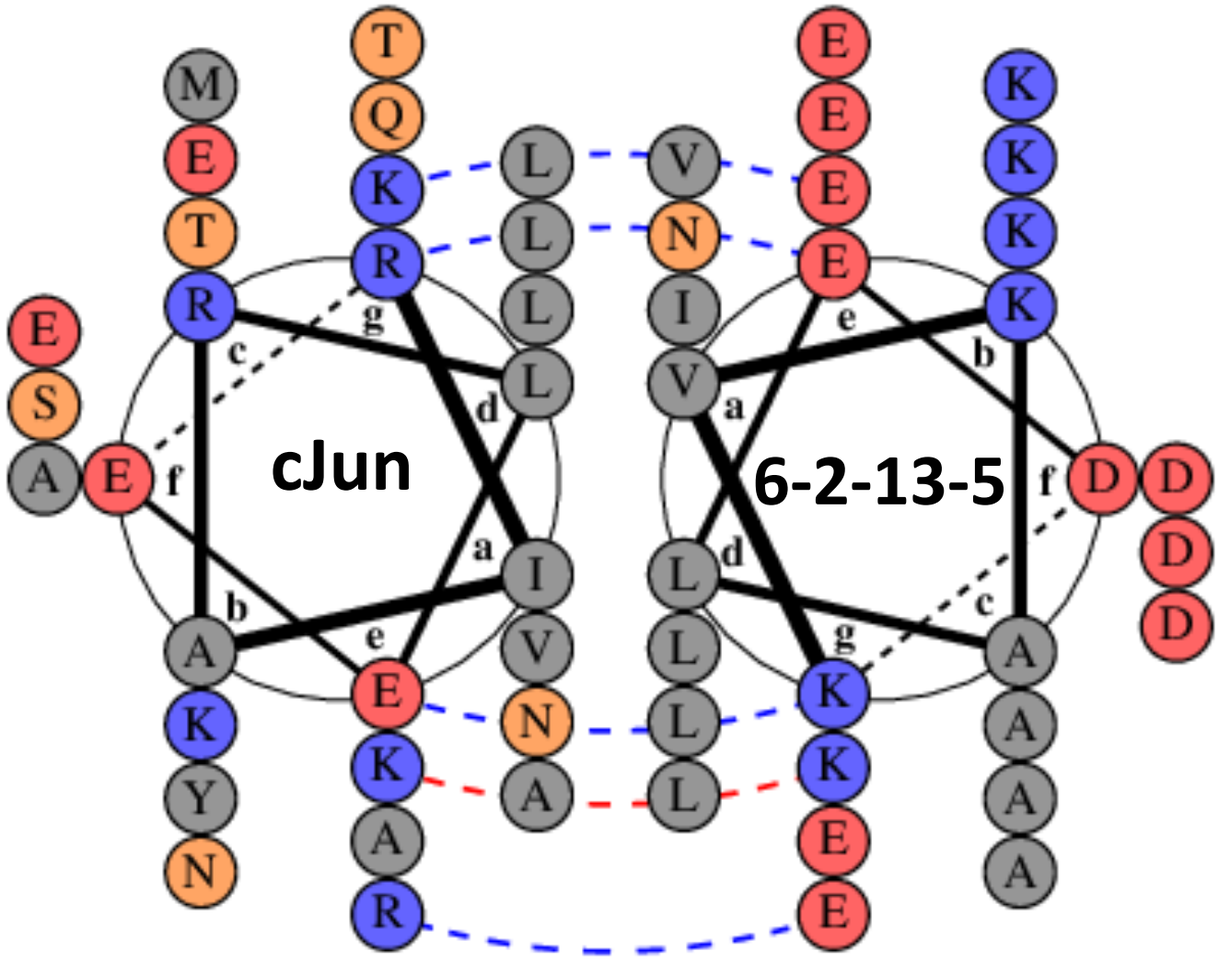

(C)

1-3-16-7: YEIKALEDELKALEDKNKALKDEIKALKD

6-2-13-5: YKVKALEDKIKALEDENKALEDEVKALED

Figure 5

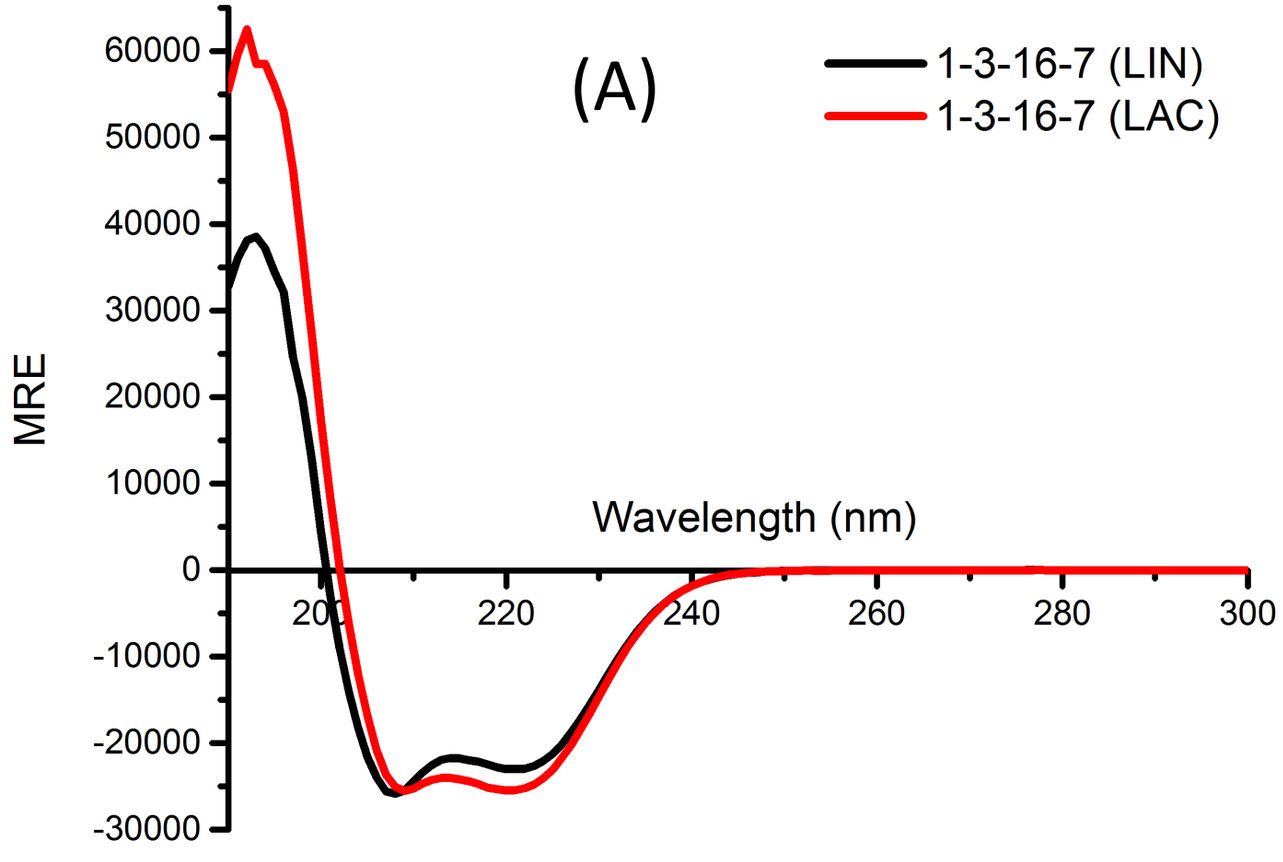
(A)
1-3-16-7 (LIN)
1-3-16-7 (LAC)
MRE
Wavelength (nm)
60000
50000
40000
30000
20000
10000
0
-10000
-20000
-30000
200
220
240
260
280
300

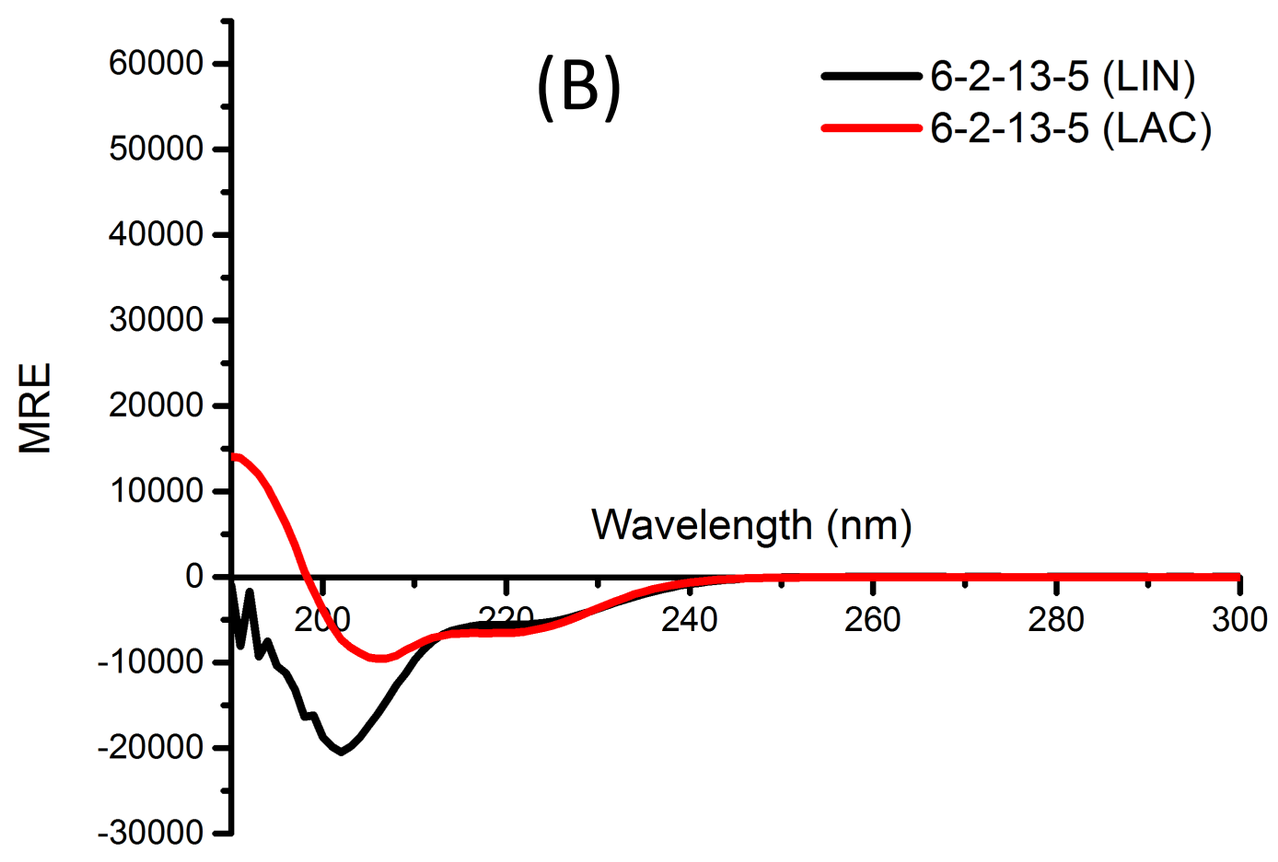
(B)
6-2-13-5 (LIN)
6-2-13-5 (LAC)
MRE
Wavelength (nm)
60000
50000
40000
30000
20000
10000
0
-10000
-20000
-30000
200
220
240
260
280
300

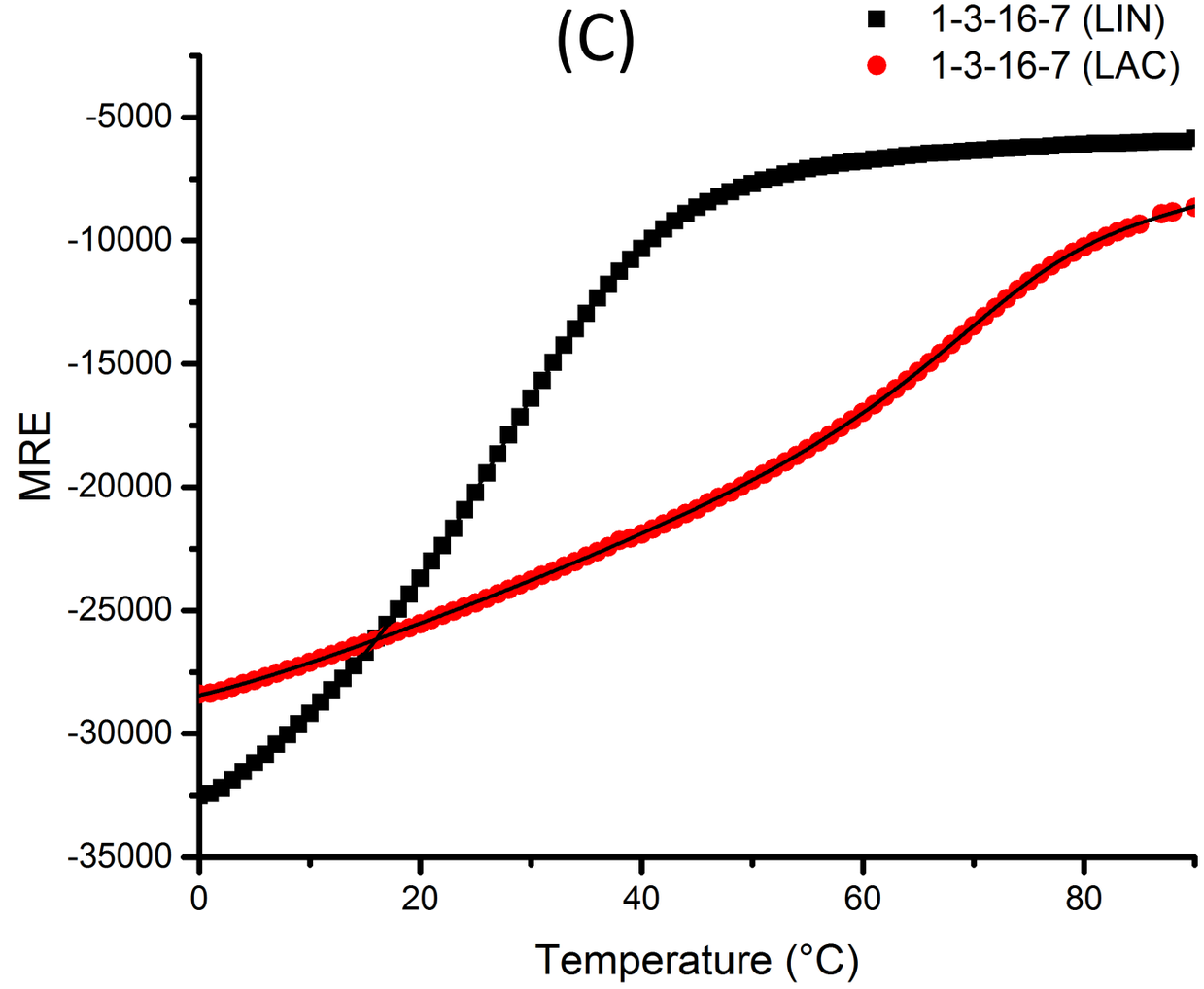
(C)
1-3-16-7 (LIN)
1-3-16-7 (LAC)
MRE
Temperature (°C)
-5000
-10000
-15000
-20000
-25000
-30000
-35000
0
20
40
60
80

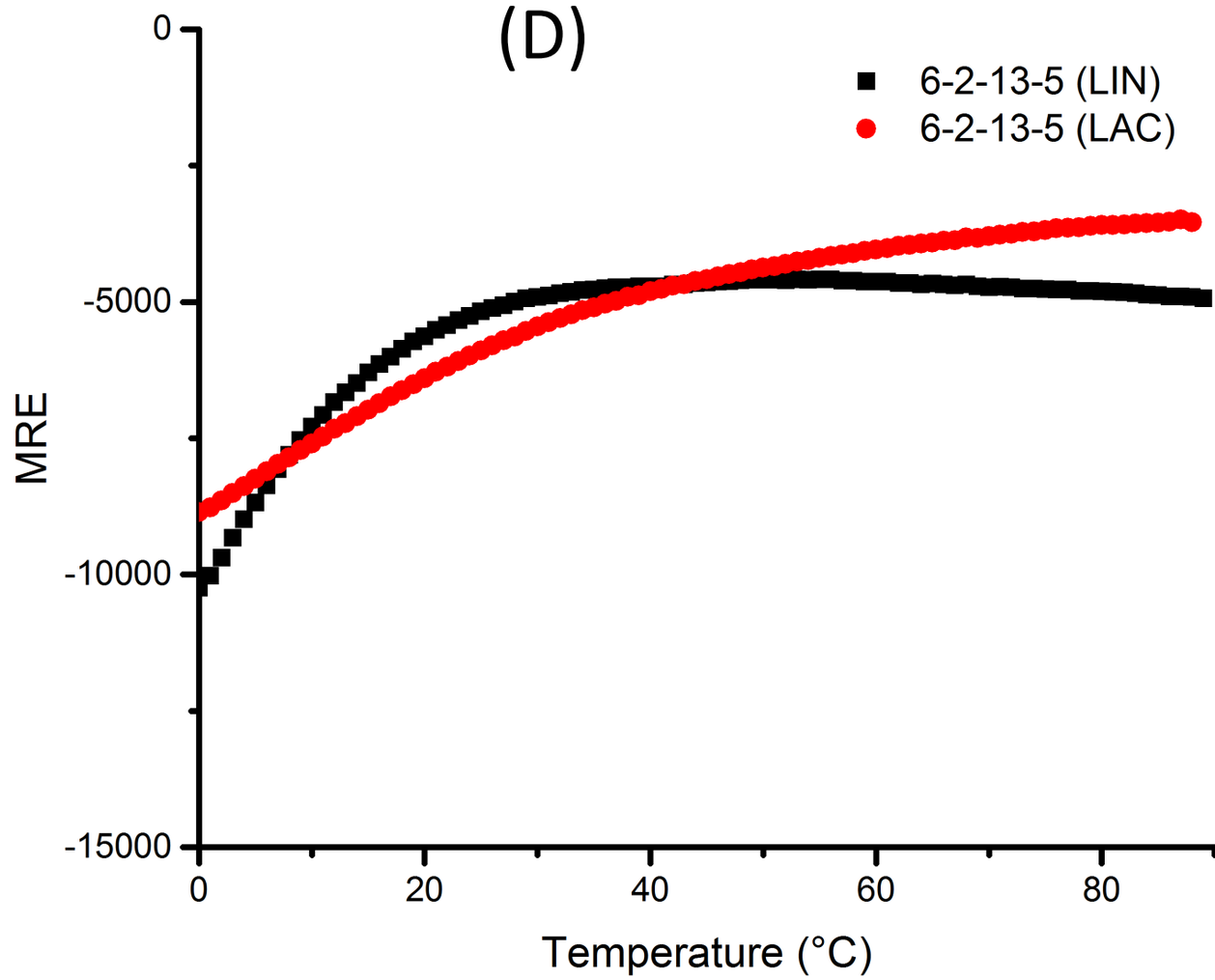
(D)
6-2-13-5 (LIN)
6-2-13-5 (LAC)
MRE
Temperature (°C)
0
-5000
-10000
-15000
0
20
40
60
80

Figure 6

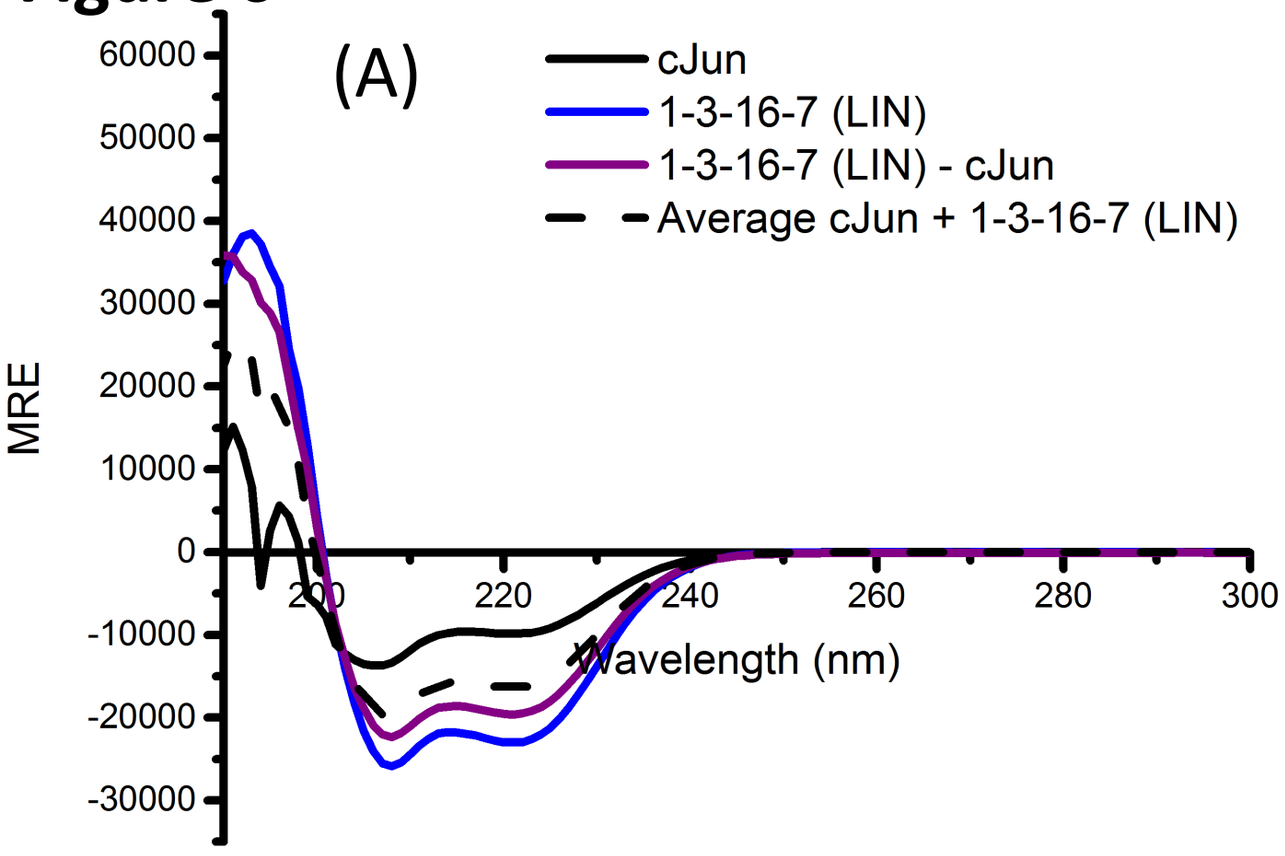
(A)
cJun
1-3-16-7 (LIN)
1-3-16-7 (LIN) - cJun
Average cJun + 1-3-16-7 (LIN)
MRE
60000
50000
40000
30000
20000
10000
0
-10000
-20000
-30000
200
220
240
260
280
300
Wavelength (nm)

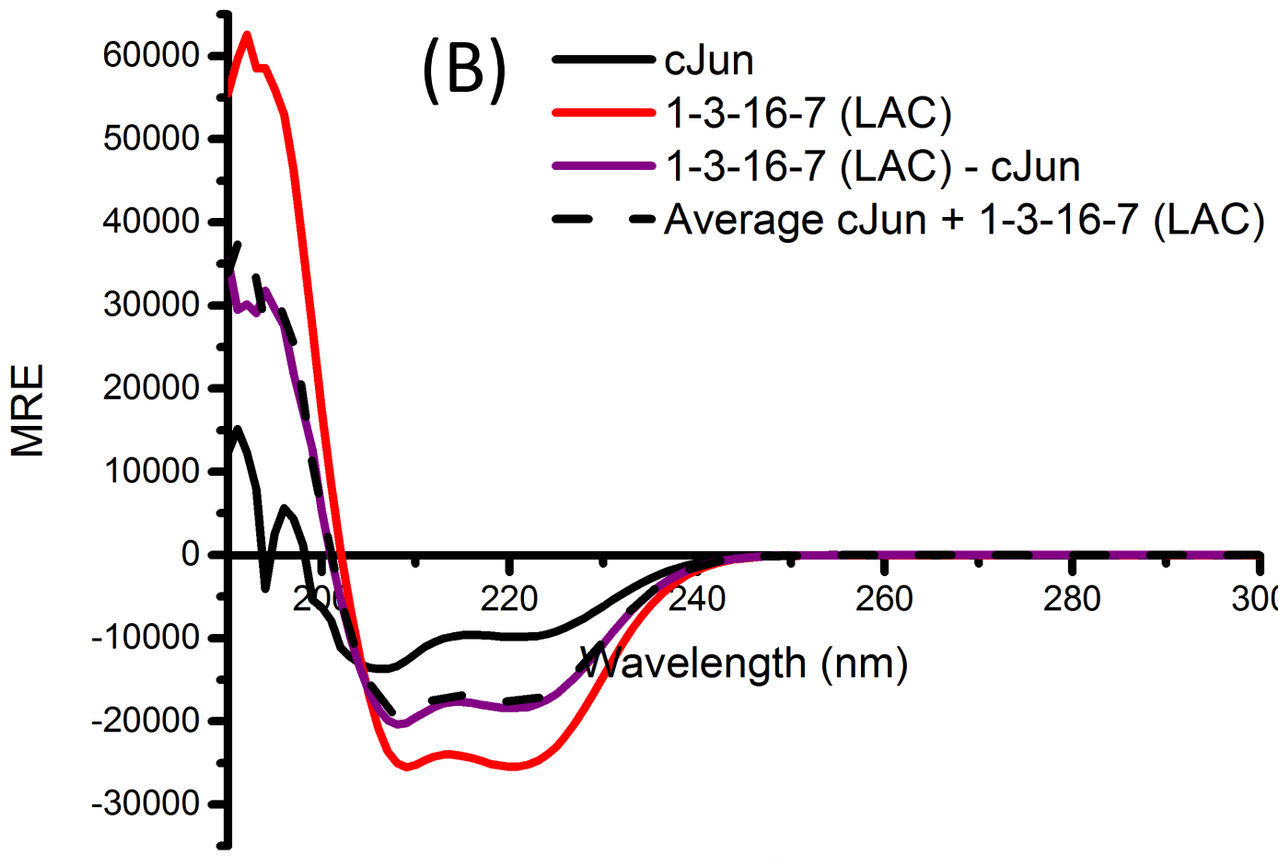
(B)
cJun
1-3-16-7 (LAC)
1-3-16-7 (LAC) - cJun
Average cJun + 1-3-16-7 (LAC)
MRE
60000
50000
40000
30000
20000
10000
0
-10000
-20000
-30000
220
240
260
280
Wavelength (nm)

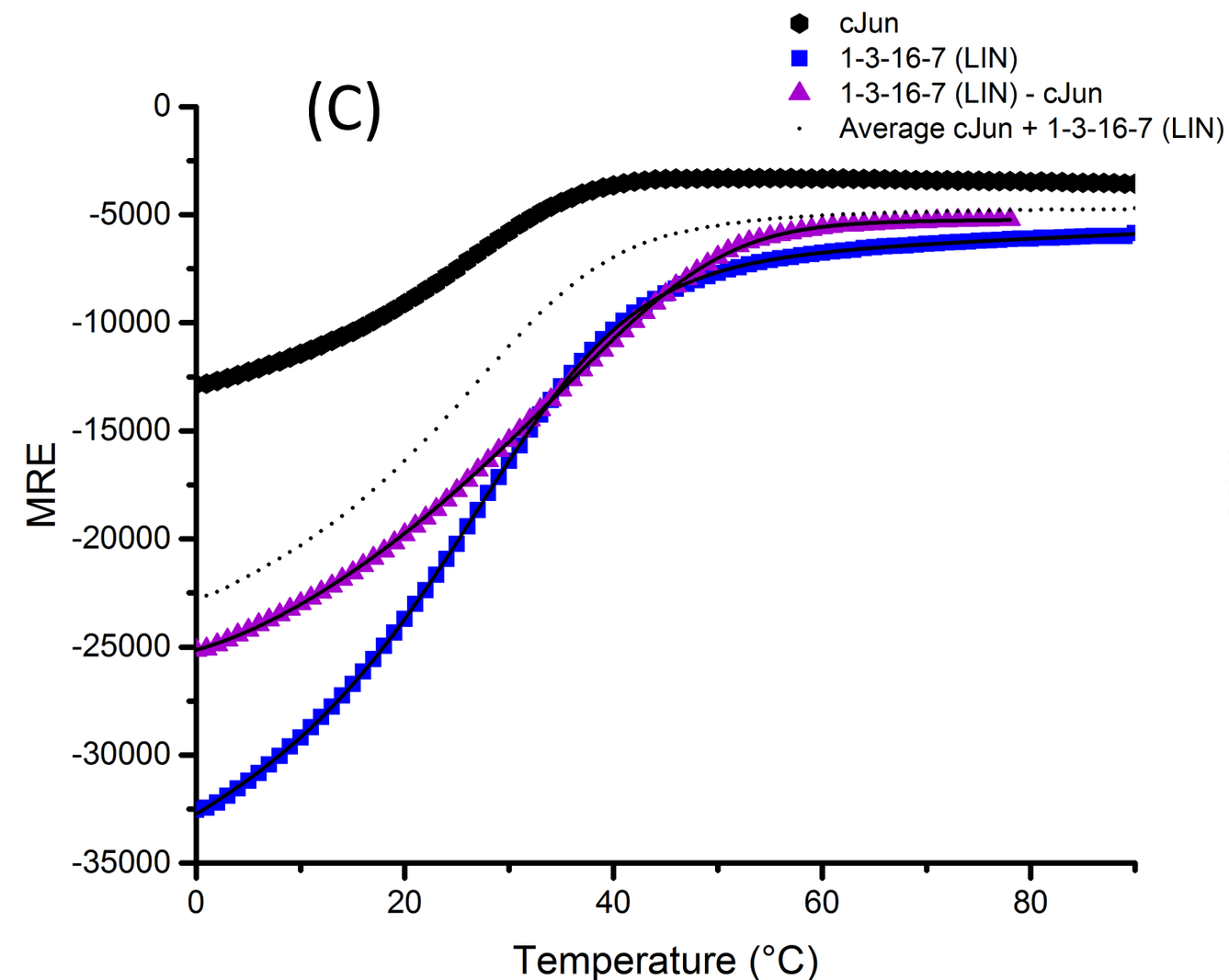
(C)
cJun
1-3-16-7 (LIN)
1-3-16-7 (LIN) - cJun
Average cJun + 1-3-16-7 (LIN)
MRE
0
-5000
-10000
-15000
-20000
-25000
-30000
-35000
0
20
40
60
80
Temperature (°C)

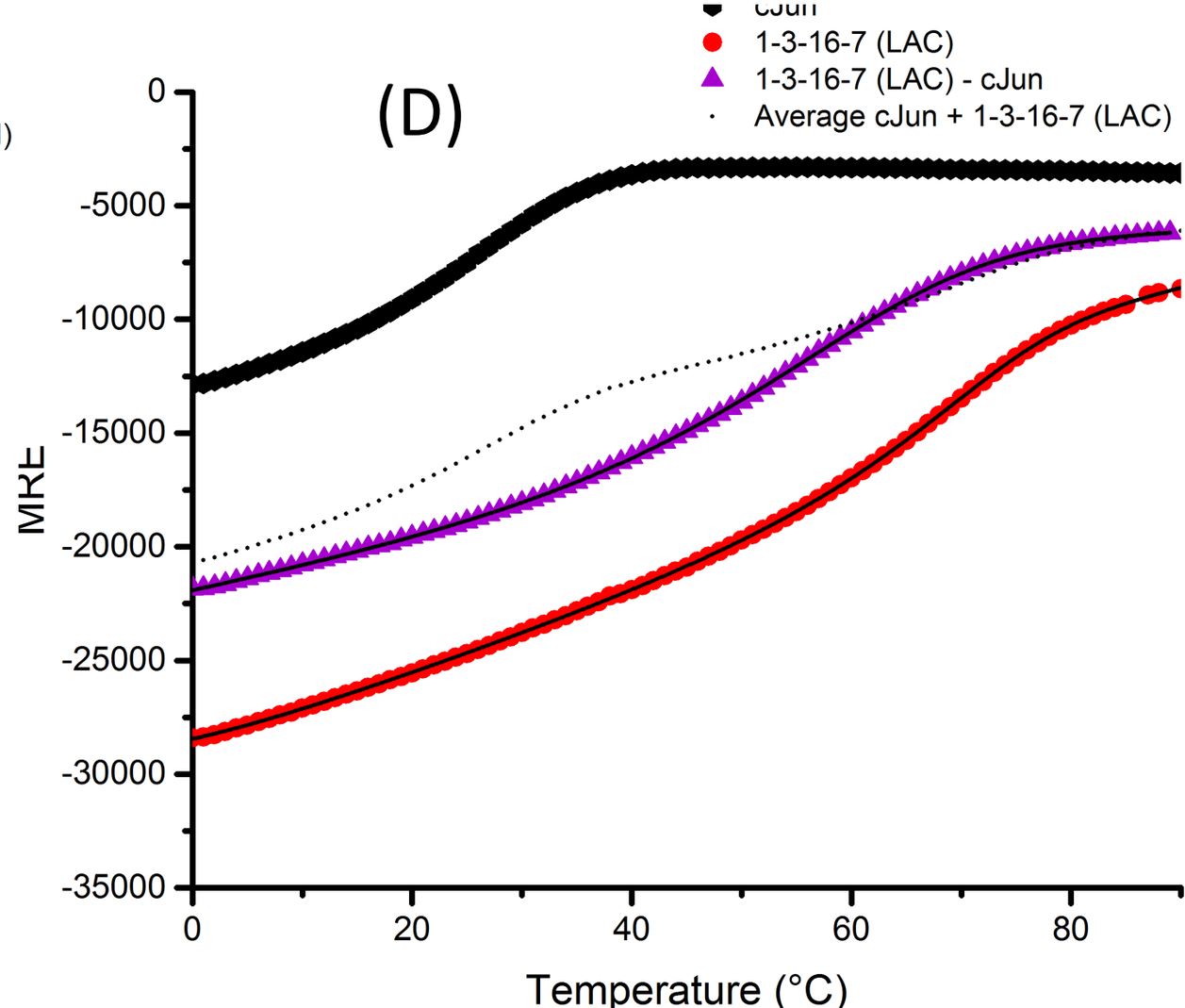
(D)
cJun
1-3-16-7 (LAC)
1-3-16-7 (LAC) - cJun
Average cJun + 1-3-16-7 (LAC)
MRE
0
-5000
-10000
-15000
-20000
-25000
-30000
-35000
0
20
40
60
80
Temperature (°C)

Figure 7

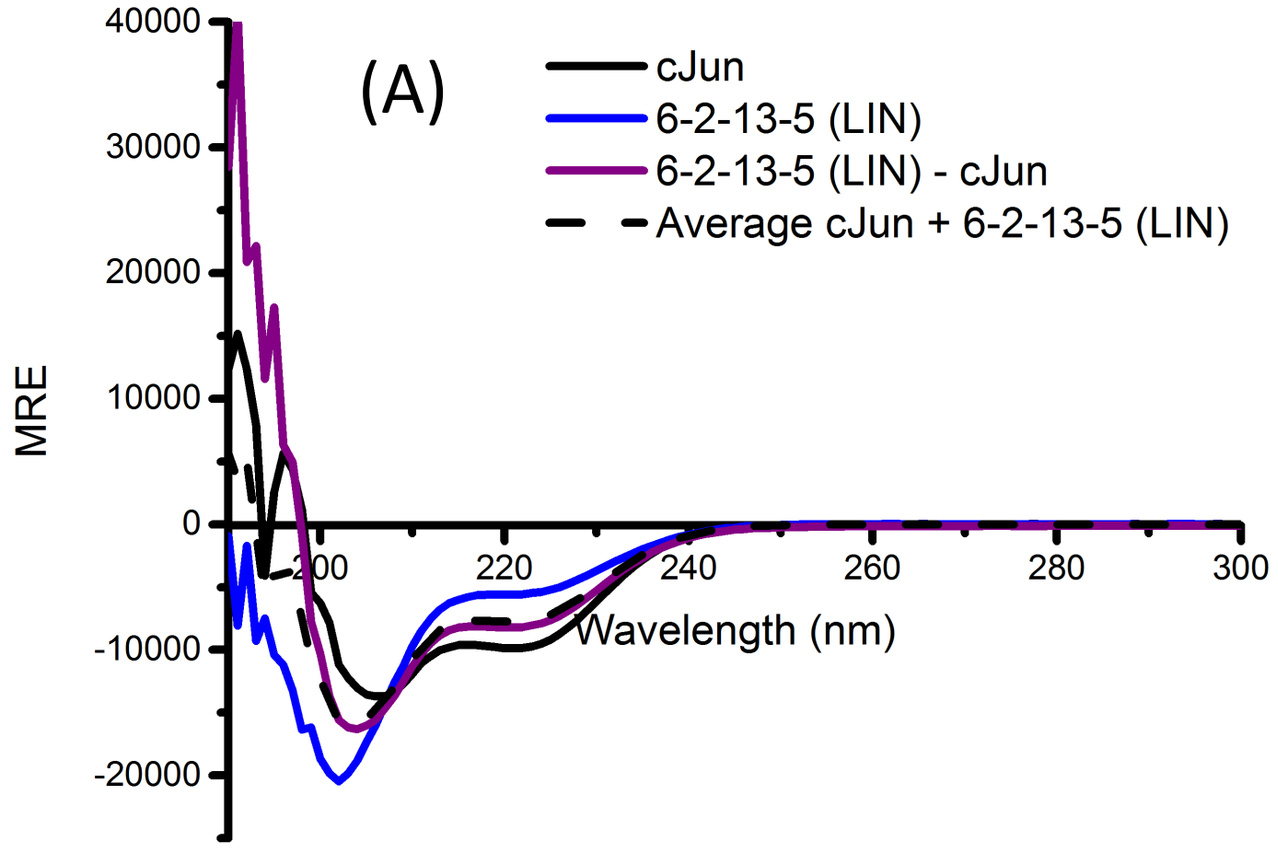
(A)
cJun
6-2-13-5 (LIN)
6-2-13-5 (LIN) - cJun
Average cJun + 6-2-13-5 (LIN)
MRE
Wavelength (nm)

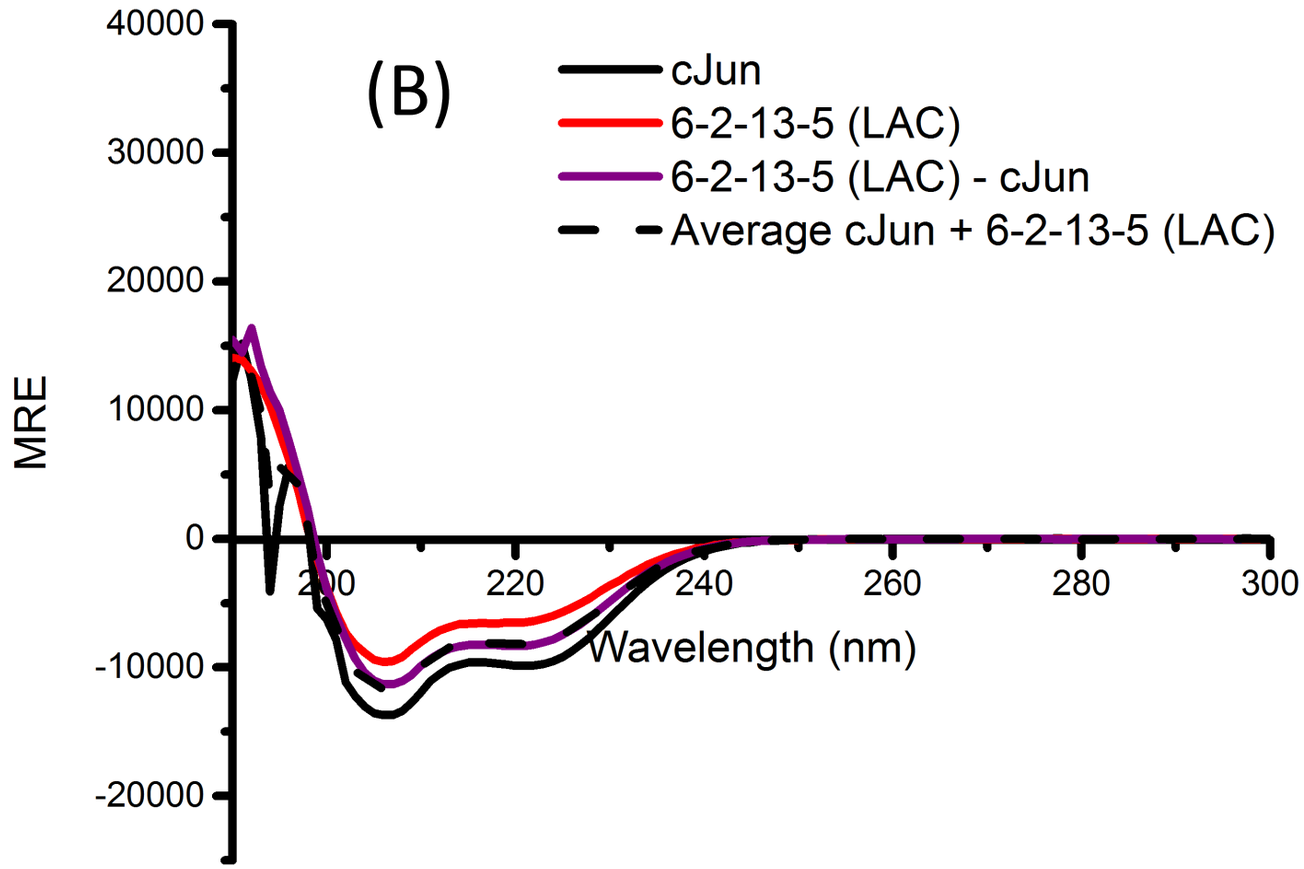
(B)
cJun
6-2-13-5 (LAC)
6-2-13-5 (LAC) - cJun
Average cJun + 6-2-13-5 (LAC)
MRE
Wavelength (nm)

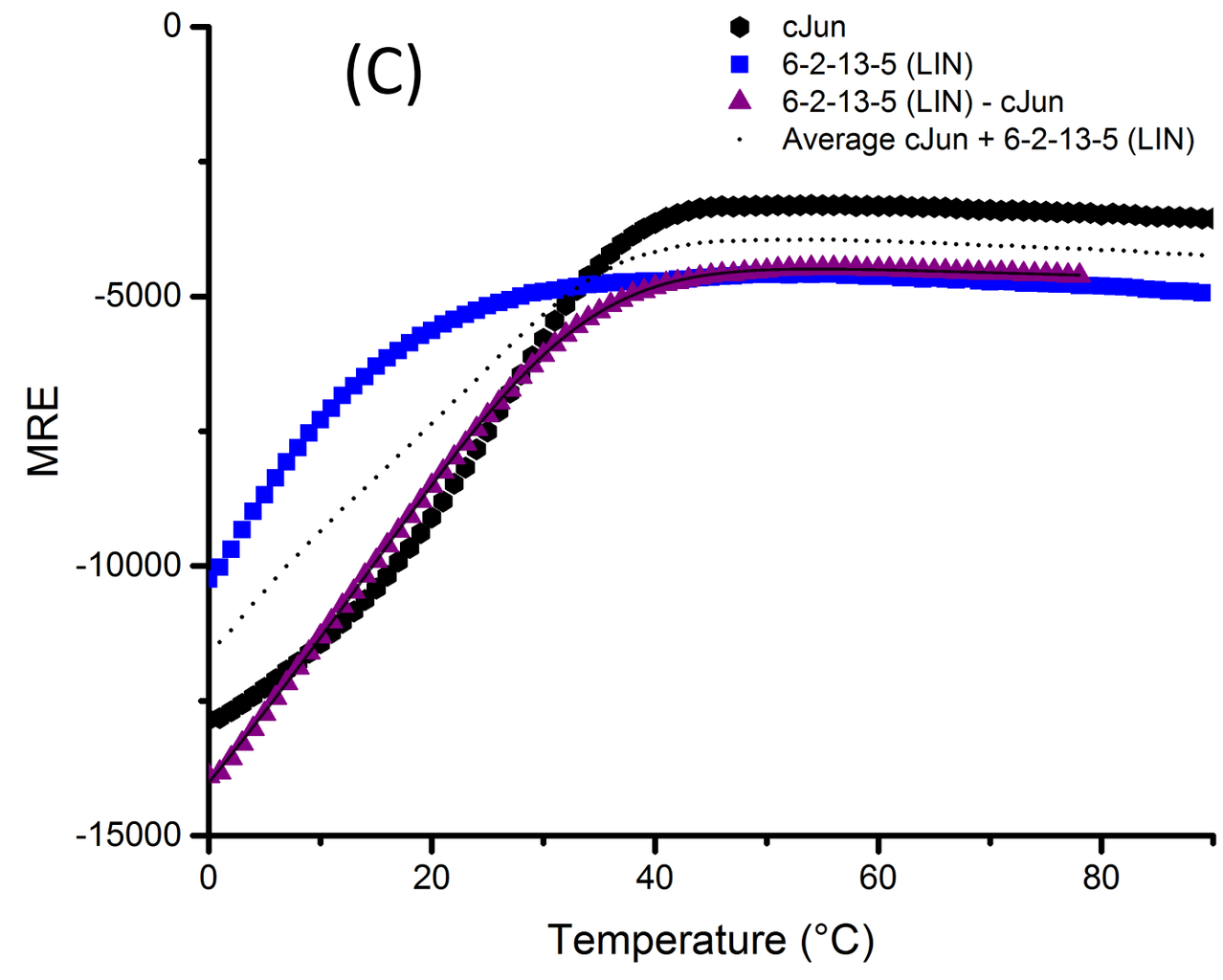
(C)
cJun
6-2-13-5 (LIN)
6-2-13-5 (LIN) - cJun
Average cJun + 6-2-13-5 (LIN)
MRE
Temperature (°C)

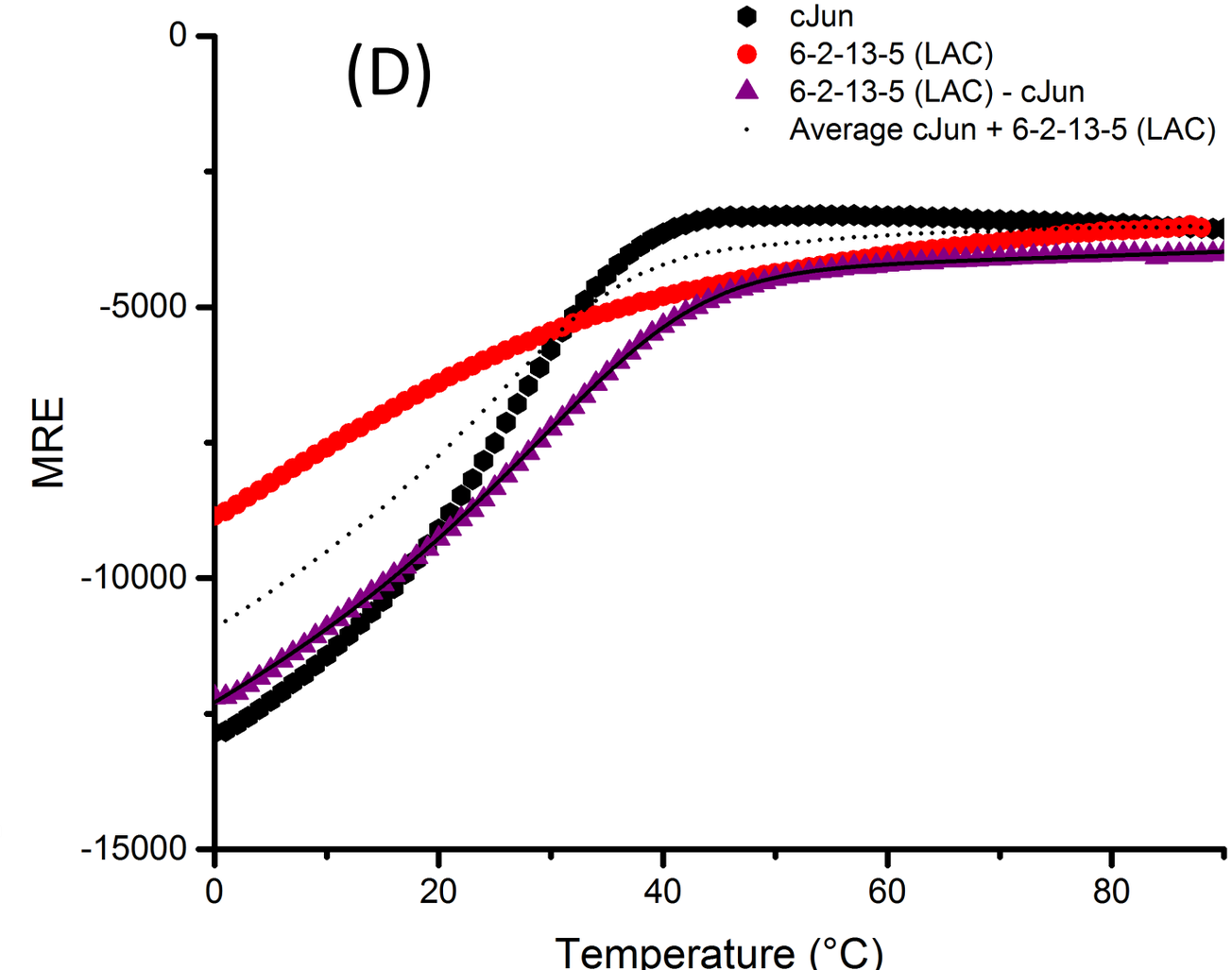
(D)
cJun
6-2-13-5 (LAC)
6-2-13-5 (LAC) - cJun
Average cJun + 6-2-13-5 (LAC)
MRE
Temperature (°C)

Figure 8

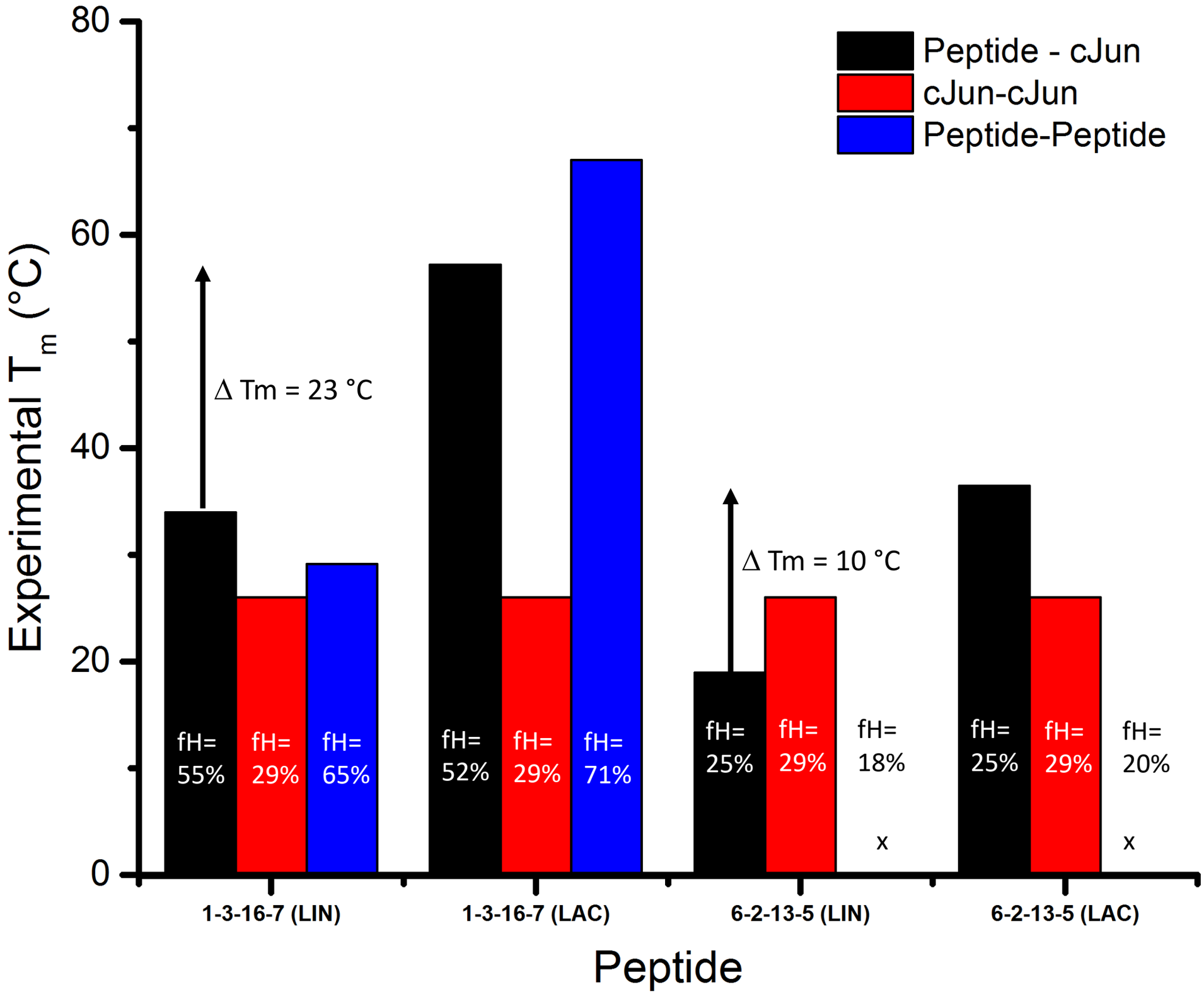
Peptide - cJun
cJun-cJun
Peptide-Peptide
Experimental T_m (°C)
80
60
40
20
0
Δ Tm = 23 °C
Δ Tm = 10 °C
fH= 55%
fH= 29%
fH= 65%
fH= 52%
fH= 29%
fH= 71%
fH= 25%
fH= 29%
fH= 18%
x
fH= 25%
fH= 29%
fH= 20%
x
1-3-16-7 (LIN)
1-3-16-7 (LAC)
6-2-13-5 (LIN)
6-2-13-5 (LAC)
Peptide

Figure 9

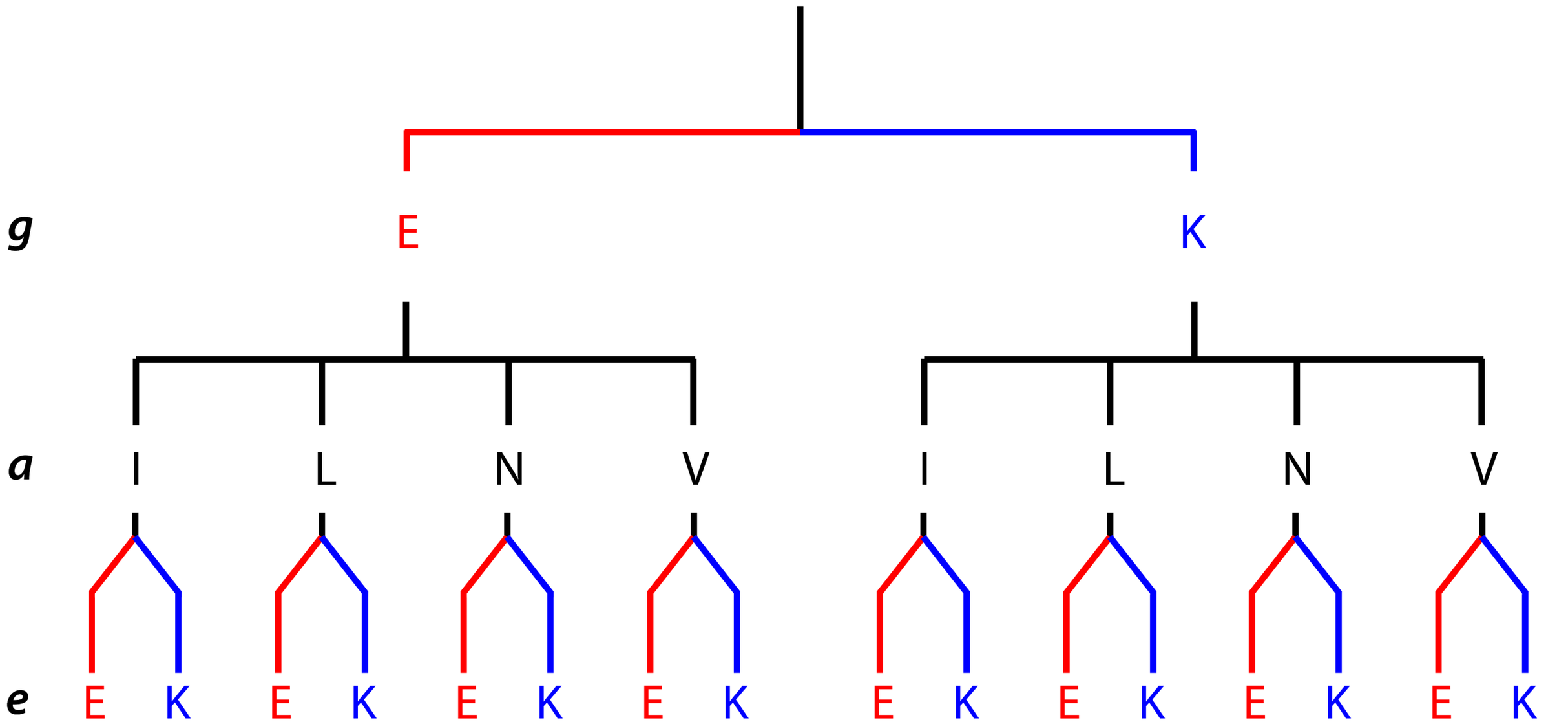
g
E
K
a
I
L
N
V
I
L
N
V
e
E
K
E
K
E
K
E
K
E
K
E
K
E
K
E
K
45%
68%
60%
57%
47%
49%
41%
62%
34%
41%
35%
47%
45%
55%
36%
49%
C1
C7
C3
C9
C13
C15
C5
C11
C2
C8
C4
C10
C14
C16
C6
C12

Table 1. The Comparative Helicity of Cassettes 1-16

Cassette Number	Sequence *gabcdef* ga**K**AL*e***D**	Linear fH (%)	Cyclic fH (%)	ΔfH (%)
1	(Y)*EI***K**AL*E***D**	10.8	45.0	34.2
2	(Y)*KI***K**AL*E***D**	10.8	34.4	23.5
3	(Y)*EL***K**AL*E***D**	10.4	60.3	49.9
4	(Y)*KL***K**AL*E***D**	4.1	35.3	31.2
5	(Y)*EV***K**AL*E***D**	9.3	41.4	32.1
6	(Y)*KV***K**AL*E***D**	7.9	35.9	28.0
7	(Y)*EI***K**AL*K***D**	17.6	67.5	49.9
8	(Y)*KI***K**AL*K***D**	18.6	41.1	22.6
9	(Y)*EL***K**AL*K***D**	14.8	57.0	42.2
10	(Y)*KL***K**AL*K***D**	6.2	47.4	41.2
11	(Y)*EV***K**AL*K***D**	12.6	62.2	49.6
12	(Y)*KV***K**AL*K***D**	8.0	48.7	40.7
13	(Y)*EN***K**AL*E***D**	14.7	46.7	32.0
14	(Y)*KN***K**AL*E***D**	7.4	44.8	37.4
15	(Y)*EN***K**AL*K***D**	12.4	49.1	36.7
16	(Y)*KN***K**AL*K***D**	4.5	55.1	50.6

Table 2. Selection of Cassettes For Conjugation

RIARLEE			*KVKTLKA*			*QNYELAS*			*TANMLRE*		
Heptad 1			**Heptad 2**			**Heptad 3**			**Heptad 4**		
Cassette	**Heterodimer T_m (°C)**	**Helicity (%)**	**Cassette**	**Heterodimer T_m (°C)**	**Helicity (%)**	**Cassette**	**Heterodimer T_m (°C)**	**Helicity (%)**	**Cassette**	**Heterodimer T_m (°C)**	**Helicity (%)**
2	31.1	34.4%	1	47.2	45.0%	1	12.5	45.0%	3	27.6	60.3%
6	29.8	35.9%	3	44.8	60.3%	7	10.7	67.5%	1	24.7	45.0%
4	28.7	35.3%	5	40.6	41.4%	3	10.2	60.3%	5	23.4	41.4%
1	25.8	45.0%	2	33.4	34.4%	13	8.7	46.7%	9	23.4	57.0%
5	24.5	41.4%	7	33.4	67.5%	9	8.4	57.0%	7	20.5	67.5%
3	23.4	60.3%	4	31.0	35.3%	2	8.4	34.4%	11	19.2	62.2%
8	19.8	41.1%	9	31.0	57.0%	15	6.9	49.1%	4	16.2	35.3%
12	18.5	48.7%	13	27.5	46.7%	8	6.6	41.1%	13	15.5	46.7%
10	17.4	47.4%	11	26.9	62.2%	4	6.0	35.3%	2	13.3	34.4%
14	16.7	44.8%	6	26.9	35.9%	5	6.0	41.4%	10	12.0	47.4%
7	14.4	67.5%	8	19.7	41.1%	14	4.5	44.8%	6	12.0	35.9%
11	13.1	62.2%	10	17.3	47.4%	10	4.2	47.4%	15	11.3	49.1%
9	12.0	57.0%	14	13.7	44.8%	11	4.2	62.2%	8	9.1	41.1%
13	11.3	46.7%	15	13.7	49.1%	16	2.7	55.1%	12	7.8	48.7%
16	5.4	55.1%	12	13.1	48.7%	6	1.8	35.9%	14	4.2	44.8%
15	0.0	49.1%	16	0.0	55.1%	12	0.0	48.7%	16	0.0	55.1%

Combining Constrained Heptapeptide Cassettes With Computational Design to Create Coiled-coil Targeting Helical Peptides

Alexander Lathbridge[1] and Jody M. Mason[1,2]

[1]Dept of Biology and Biochemistry, University of Bath, Claverton Down, Bath BA2 7AY

[2]To whom correspondence should be addressed: j.mason@bath.ac.uk

Running title: Heptapeptide cassettes

**Corresponding author: Jody M. Mason (E: j.mason@bath.ac.uk; T: +441225386867)*

Keywords: Coiled coil; Peptide antagonist, peptide cassettes, constrained peptides; heptads; Activator Protein-1; transcription factor.

Supporting Information

Electrospray Mass Spectroscopy Data of Linear and Lactamised Peptides – All 32 peptides provided an excellent agreement between the expected and observed mass in both linear and lactamised versions of peptide (Figure S1, peptides 1-4; Figure S2, Peptides 5-8; Figure S3, peptides 9-12; Figure S4, peptides 13-16).

Peptide Sequences - All synthesised and characterised peptides were amidated and acetylated.

cJun: ASRIARLEEKVKTLKAQNYELASTANMLREQVAQLKGAP

1-3-16-7: YEIKALEDELKALEDKNKALKDEIKALKD

6-2-13-5: YKVKALEDKIKALEDENKALEDEVKALED

Sequence Specificity - All cassettes exhibited an increase in helicity when lactamised. However, the extent of helical gain varied, with the ability of certain residues to tolerate lactamisation over others being less clear (Fig S5-S6). As shown in Figure 3b, a wide range of fH increase due to lactamisation was observed. Since the possible amino acids combinations at ***a/e/g*** positions were limited, only partial interpretations can be drawn from the electrostatic and core configurations in optimising cassette stability. This does however present an opportunity to optimise the computational techniques employed. As previously shown,[1] bCIPA is capable of being trained on a specific subset of coiled coil forming sequences. With further experimental exploration of the cassette library, it may be possible to extract the predictors and develop a more specific prediction algorithm for this use.

Conjugated Peptide Lactamisation - As shown in Figures S7 and S8, both of the peptides exhibited a decrease in mass of 36 Da, indicating that both lactam bridges successfully formed between Asp and Lys, resulting in the loss of two water molecules.

Although peptides truncated less than 29 residues have been explored previously[2–7] with a focus on maintaining stability, it was decided to conjugate four cassettes to maximise the potential interpretation and to maintain a quantifiable stability with the target.

Table S1. Electrospray Mass Spectroscopy Data of Linear and Lactamised Peptides

Peptide	Sequence	**Expected Linear Mass**	**Observed Linear Mass**	**Expected Cyclic Mass**	**Observed Cyclic Mass**	**Mass Change Linear — Cyclic**
1	YEIKALED	1021.50	**1021.53**	1003.50	**1003.52**	18.01
2	YKIKALED	1020.55	**1020.58**	1002.55	**1002.57**	18.01
3	YELKALED	1021.50	**1021.53**	1003.50	**1003.53**	18.00
4	YKLKALED	1021.50	**1020.58**	1003.50	**1002.57**	18.01
5	YEVKALED	1007.48	**1007.51**	989.48	**989.51**	18.00
6	YKVKALED	1006.53	**1006.56**	988.53	**988.56**	18.00
7	YEIKALKD	1020.55	**1020.57**	1002.55	**1002.57**	18.00
8	YKIKALKD	1019.60	**1019.62**	1001.60	**1001.62**	18.00
9	YELKALKD	1020.55	**1020.58**	1002.55	**1002.57**	18.01
10	YKLKALKD	1019.60	**1019.62**	1001.60	**1001.62**	18.01
11	YEVKALKD	1006.53	**1006.57**	988.53	**988.55**	18.01
12	YKVKALKD	1005.59	**1005.61**	987.59	**987.61**	18.01
13	YENKALED	1022.46	**1022.48**	1004.46	**1004.48**	18.00
14	YKNKALED	1021.51	**1021.53**	1003.51	**1003.52**	18.01
15	YENKALKD	1021.51	**1021.53**	1003.51	**1003.53**	18.01
16	YKNKALKD	1020.56	**1020.59**	1002.56	**1002.58**	18.01

Mass spectrometry data for cassettes 1-16. For each peptide the predicted mass, observed mass for both linear and cyclic forms of each cassette are shown. As expected, the difference between the linear and lactamised form of the cassette accounts for the loss of one water molecule in every case.

Table S2. Helical and Thermal Stability of Linear and Lactamised Peptides

Peptide	fH (%)	222 nm/208 nm	T_m (°C)
cJun	29.1	0.73	25.7
1-3-16-7 Linear	65.3	0.89	29.13
1-3-16-7 Lactamised	71.4	1.01	67
6-2-13-5 Linear	18.2	0.44	N/A
6-2-13-5 Lactamised	20.4	0.69	N/A
1-3-16-7 Linear : cJun	55.2	0.87	34
1-3-16-7 Lactamised : cJun	52.0	0.90	57.2
6-2-13-5 Linear : cJun	24.9	0.60	18.9
6-2-13-5 Lactamised : cJun	25.0	0.74	29.2

A comparison of the full length peptide complexes – with their fractional helicty, 222 nm/208 nm ratio, and transition midpoint (T_m) values.

Computational Processing

All software was run on Python on a 64-bit x64-based processor Windows machine with 12 GB of RAM as described previously[1].

Figure S1. **Electrospray Mass Spectrometry data from the purified cassettes 1-4** demonstrating a loss of 18 Da between the linear and successfully lactamised forms of cassette 1 (A/B), cassette 2 (C/D), cassette 3 (E/F), and cassette 4 (G/H).

Figure S2. **Electrospray Mass Spectrometry data from the purified cassettes 5-8** demonstrating a loss of 18 Da between the linear and successfully lactamised forms of cassette 5 (A/B), cassette 6 (C/D), cassette 7 (E/F), and cassette 8 (G/H).

Figure S3. **Electrospray Mass Spectrometry data from the purified cassettes 9-12** demonstrating a loss of 18 Da between the linear and successfully lactamised forms of cassette 9 (A/B), cassette 10 (C/D), cassette 11 (E/F), and cassette 12 (G/H).

Figure S4. **Electrospray Mass Spectrometry data from the purified cassettes 13-16** demonstrating a loss of 18 Da between the linear and successfully lactamised forms of cassette 13 (A/B), cassette 14 (C/D), cassette 15 (E/F), and cassette 16 (G/H).

Figure S5. **Thermal spectra for cassettes 1-16 in linear form.** Spectra were initially measured at 20 °C (black) and in 10°C increments to 90°C (red) and then post melt at 20°C (blue) at a total peptide concentration of 150 µM and presented as mean residue ellipticity (MRE). All experiments were performed in 10 mM potassium phosphate and 100 mM potassium fluoride (pH 7). For all cases, the

linear forms were characterised as having a random coil profile at 20°C, both prior to thermal denaturation and as post-melt samples, with disorder persisting at 90°C.

Figure S6. Thermal spectra for cassettes 1-16 in lactamised form. Spectra were initially measured at 20 °C (black) and in 10°C increments to 90°C (red) and then post melt at 20°C (blue) at a total peptide concentration of 150 μM and presented as mean residue ellipticity (MRE). All experiments were performed in 10 mM potassium phosphate and 100 mM potassium fluoride (pH 7). In all cases, lactamised cassettes presented as α-helical at 20°C and returned to within 5% of the same helical signature as post-melt samples, with an average helicity of 48%. Consistent with lactamisation as a potent helix-inducer, at 90°C helicity was retained with an average fH of 38%.

Figure S7. Electrospray Mass Spectrometry data from the purified full-length 1-3-16-7 demonstrates the peptide to have the expected mass of 3415.91 Da as a linear sequence (A) and the expected mass of 3379.91 Da when lactamised (B). The loss of 36 Da demonstrates that there has been successful successful lactamisation at both termini consistent with the loss of two water molecules.

Figure S8. **Electrospray Mass Spectrometry data from the purified full-length 6-2-13-5** demonstrates the peptide to have the expected mass of 3388.79 Da as a linear sequence (A) and the expected mass of 3352.79 Da when lactamised (B). The loss of 36 Da demonstrates that there has been successful lactamisation at both termini consistent with the loss of two water molecules.

References

(1) Lathbridge, A., and Mason, J. M. (2018) Computational Competitive and Negative Design to Derive a Specific cJun Antagonist. *Biochemistry 57*, 6108–6118.

(2) Rao, T., Ruiz-Gómez, G., Hill, T. A., Hoang, H. N., Fairlie, D. P., and Mason, J. M. (2013) Truncated and Helix-Constrained Peptides with High Affinity and Specificity for the cFos Coiled-Coil of AP-1. *PLoS One 8*, e59415.

(3) Baxter, D., Perry, S. R., Hill, T. A., Kok, W. M., Zaccai, N. R., Brady, R. L., Fairlie, D. P., and Mason, J. M. (2017) Downsizing Proto-oncogene cFos to Short Helix-Constrained Peptides That Bind Jun. *ACS Chem. Biol. 12*, 2051–2061.

(4) Hoang, H. N., Driver, R. W., Beyer, R. L., Hill, T. A., D. de Araujo, A., Plisson, F., Harrison, R. S., Goedecke, L., Shepherd, N. E., and Fairlie, D. P. (2016) Helix Nucleation by the Smallest Known α-Helix in Water. *Angew. Chemie - Int. Ed. 55*, 8275–8279.

(5) De Araujo, A. D., Hoang, H. N., Kok, W. M., Diness, F., Gupta, P., Hill, T. A., Driver, R. W., Price, D.

A., Liras, S., and Fairlie, D. P. (2014) Comparative α-helicity of cyclic pentapeptides in water. *Angew. Chemie - Int. Ed. 53*, 6965–6969.

(6) Shepherd, N. E., Abbenante, G., and Fairlie, D. P. (2004) Consecutive cyclic pentapeptide modules form short alpha-helices that are very stable to water and denaturants. *Angew. Chemie - Int. Ed. 43*, 2687–2690.

(7) Mazzier, D., Peggion, C., Toniolo, C., and Moretto, A. (2014) Enhancement of the helical content and stability induced in a linear oligopeptide by an i, i+4 intramolecularly double stapled, overlapping, bicyclic [31, 22, 5]-(E)ene motif. *Biopolym. - Pept. Sci. Sect. 102*, 115–123.

Figure S1

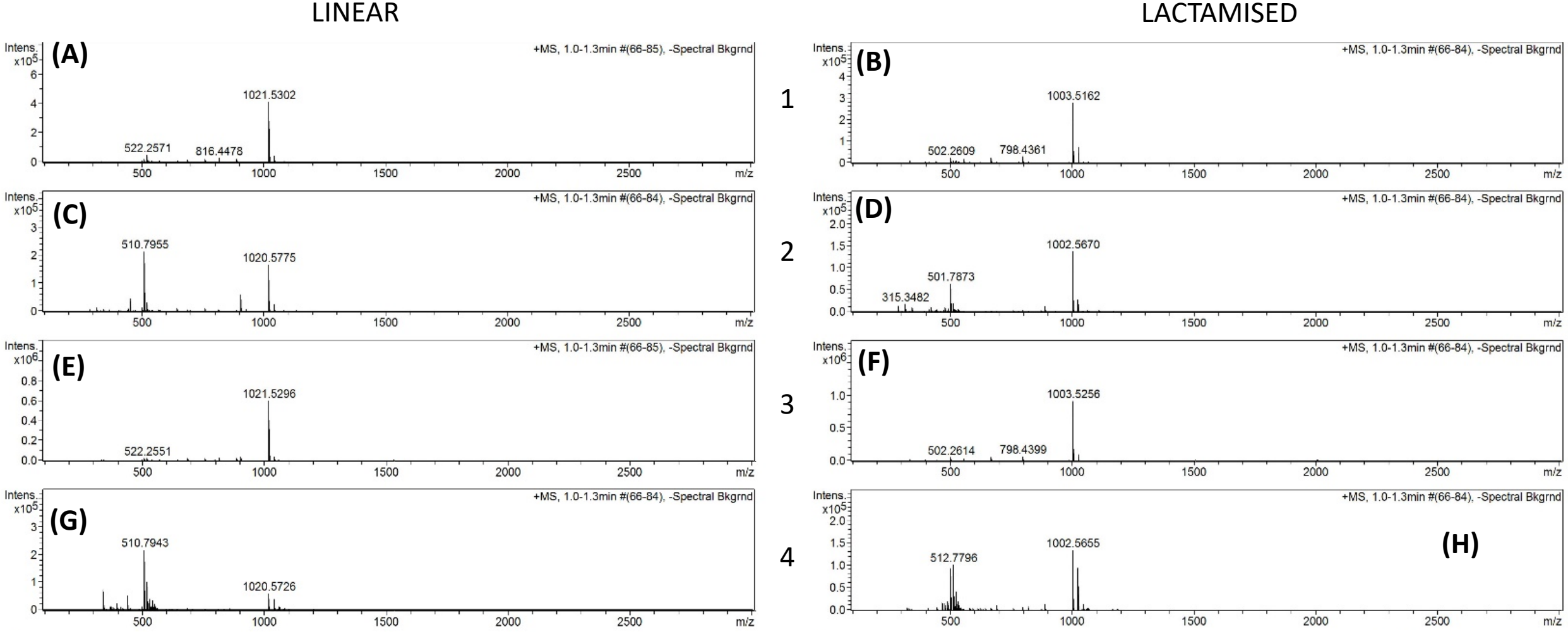
LINEAR
LACTAMISED
(A)
+MS, 1.0-1.3min #(66-85), -Spectral Bkgrnd
Intens. x10^5
1021.5302
522.2571
816.4478
(B)
+MS, 1.0-1.3min #(66-84), -Spectral Bkgrnd
Intens. x10^5
1003.5162
502.2609
798.4361
1
(C)
+MS, 1.0-1.3min #(66-84), -Spectral Bkgrnd
Intens. x10^5
510.7955
1020.5775
(D)
+MS, 1.0-1.3min #(66-84), -Spectral Bkgrnd
Intens. x10^5
1002.5670
501.7873
315.3482
2
(E)
+MS, 1.0-1.3min #(66-85), -Spectral Bkgrnd
Intens. x10^6
1021.5296
522.2551
(F)
+MS, 1.0-1.3min #(66-84), -Spectral Bkgrnd
Intens. x10^6
1003.5256
502.2614
798.4399
3
(G)
+MS, 1.0-1.3min #(66-84), -Spectral Bkgrnd
Intens. x10^5
510.7943
1020.5726
(H)
+MS, 1.0-1.3min #(66-84), -Spectral Bkgrnd
Intens. x10^5
1002.5655
512.7796
4
m/z

Figure S2

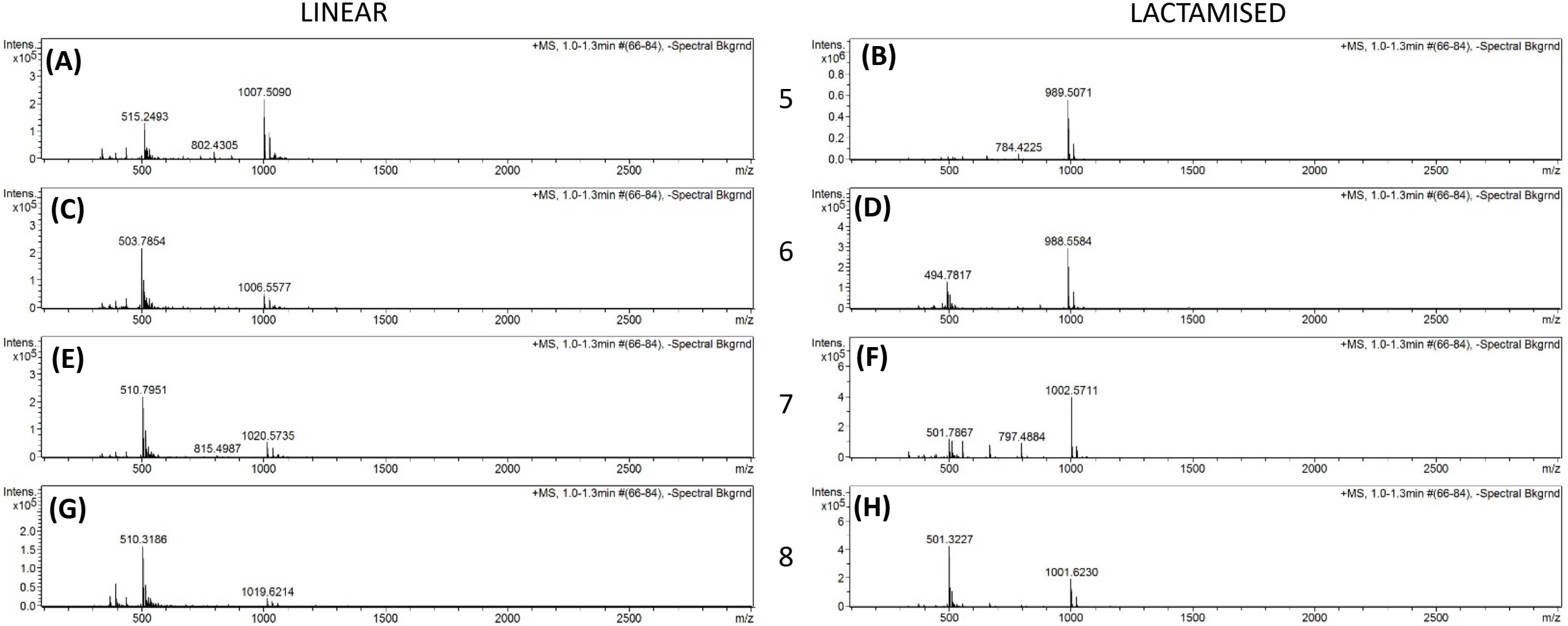
LINEAR
LACTAMISED
(A)
+MS, 1.0-1.3min #(66-84), -Spectral Bkgrnd
Intens. x10^5
1007.5090
515.2493
802.4305
m/z
(B)
Intens. x10^6
989.5071
784.4225
5
(C)
Intens. x10^5
503.7854
1006.5577
(D)
Intens. x10^5
988.5584
494.7817
6
(E)
Intens. x10^5
510.7951
1020.5735
815.4987
(F)
Intens. x10^5
1002.5711
501.7867
797.4884
7
(G)
Intens. x10^5
510.3186
1019.6214
(H)
Intens. x10^5
501.3227
1001.6230
8

Figure S3

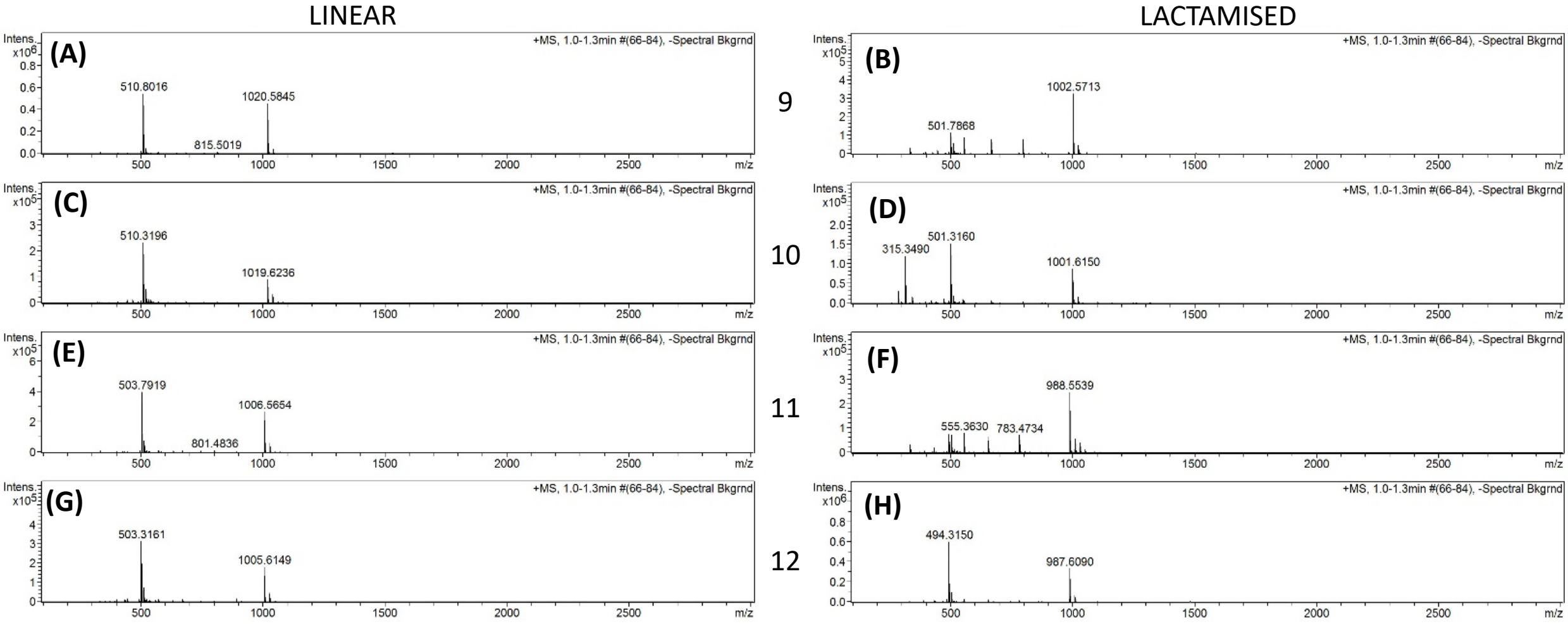
LINEAR
LACTAMISED
(A)
+MS, 1.0-1.3min #(66-84), -Spectral Bkgrnd
Intens. x10^6
510.8016
1020.5845
815.5019
9
(B)
Intens. x10^5
1002.5713
501.7868
(C)
Intens. x10^5
510.3196
1019.6236
10
(D)
Intens. x10^5
501.3160
315.3490
1001.6150
(E)
Intens. x10^5
503.7919
1006.5654
801.4836
11
(F)
Intens. x10^5
988.5539
555.3630
783.4734
(G)
Intens. x10^5
503.3161
1005.6149
12
(H)
Intens. x10^6
494.3150
987.6090
m/z

Figure S4

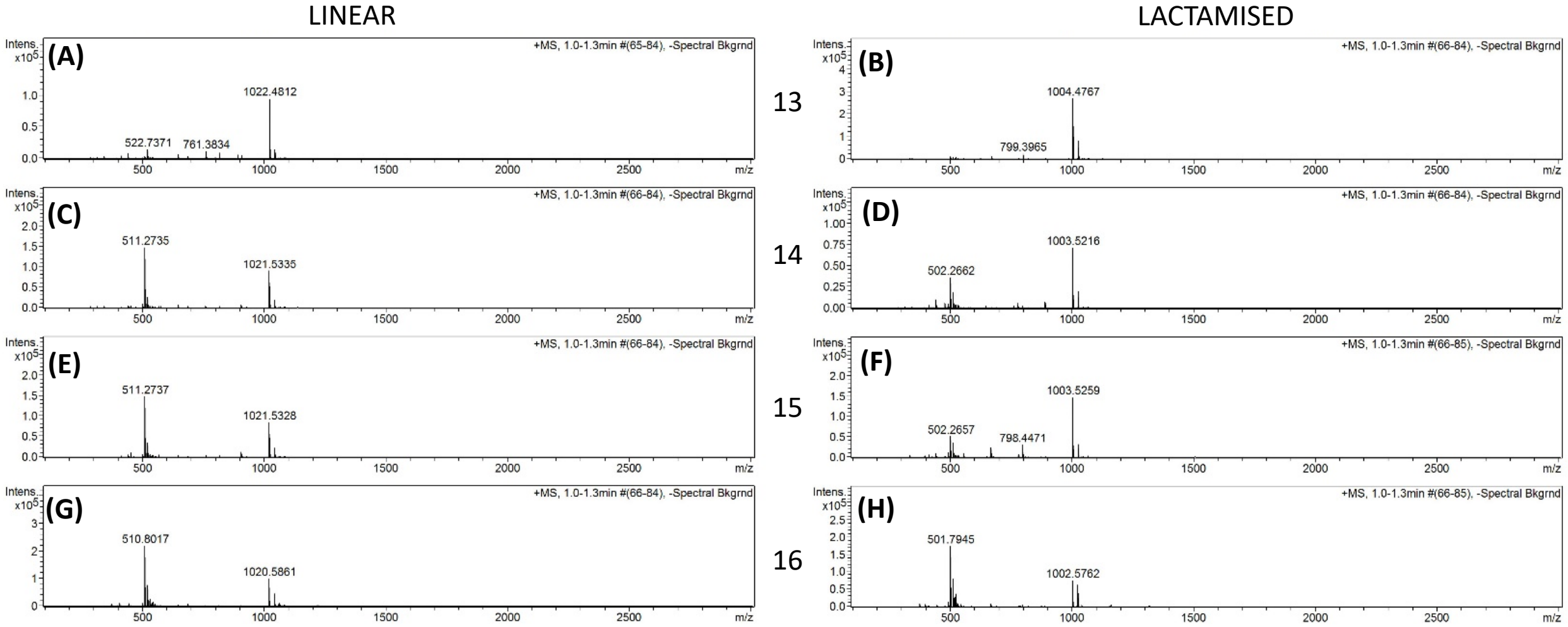
LINEAR
LACTAMISED
(A)
+MS, 1.0-1.3min #(65-84), -Spectral Bkgrnd
1022.4812
522.7371
761.3834
13
(B)
+MS, 1.0-1.3min #(66-84), -Spectral Bkgrnd
1004.4767
799.3965
(C)
+MS, 1.0-1.3min #(66-84), -Spectral Bkgrnd
511.2735
1021.5335
14
(D)
+MS, 1.0-1.3min #(66-84), -Spectral Bkgrnd
1003.5216
502.2662
(E)
+MS, 1.0-1.3min #(66-84), -Spectral Bkgrnd
511.2737
1021.5328
15
(F)
+MS, 1.0-1.3min #(66-85), -Spectral Bkgrnd
1003.5259
502.2657
798.4471
(G)
+MS, 1.0-1.3min #(66-84), -Spectral Bkgrnd
510.8017
1020.5861
16
(H)
+MS, 1.0-1.3min #(66-85), -Spectral Bkgrnd
501.7945
1002.5762
Intens.
x10^5
m/z

Figure S5

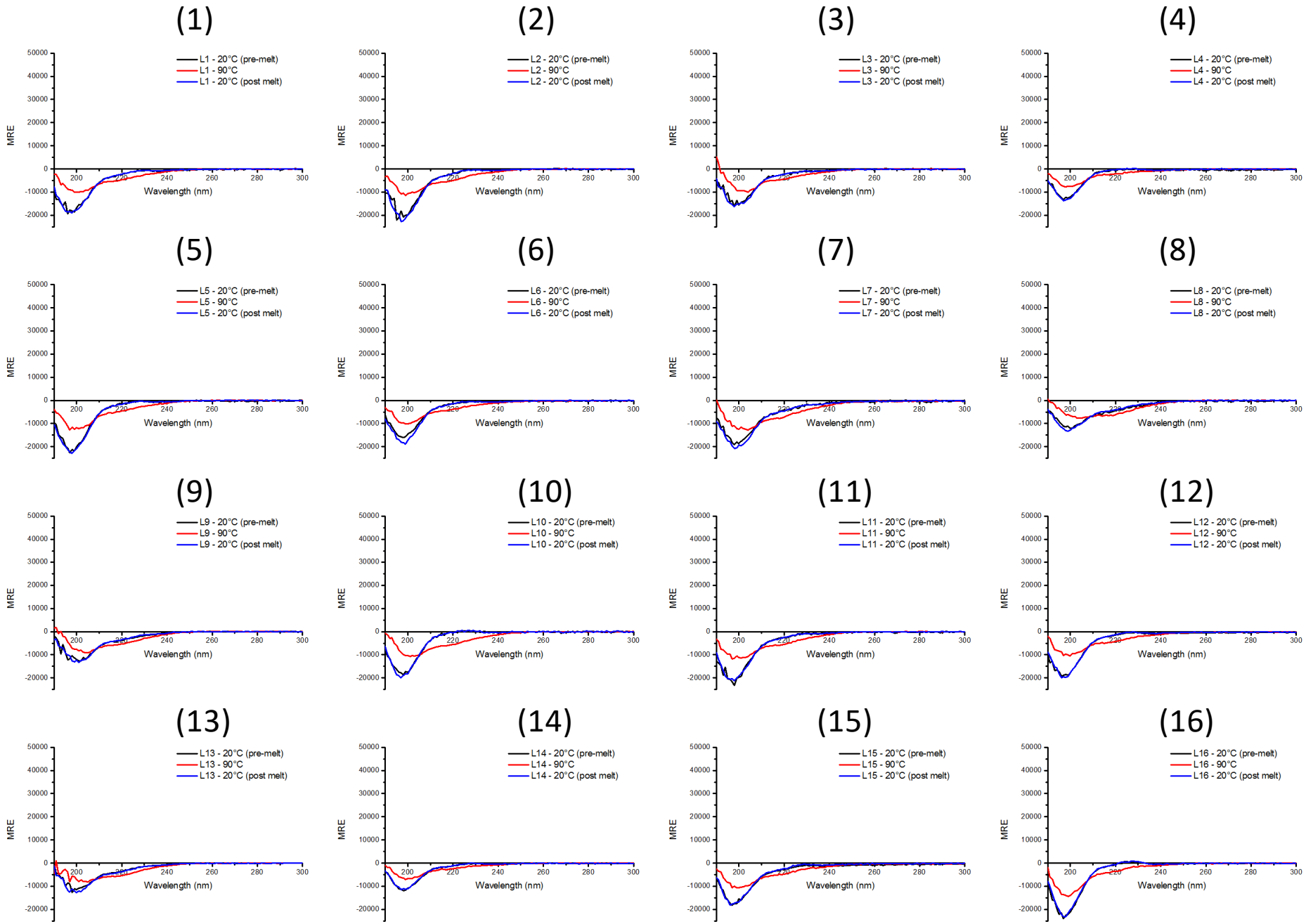
(1)
L1 - 20°C (pre-melt)
L1 - 90°C
L1 - 20°C (post melt)
(2)
L2 - 20°C (pre-melt)
L2 - 90°C
L2 - 20°C (post melt)
(3)
L3 - 20°C (pre-melt)
L3 - 90°C
L3 - 20°C (post melt)
(4)
L4 - 20°C (pre-melt)
L4 - 90°C
L4 - 20°C (post melt)
(5)
L5 - 20°C (pre-melt)
L5 - 90°C
L5 - 20°C (post melt)
(6)
L6 - 20°C (pre-melt)
L6 - 90°C
L6 - 20°C (post melt)
(7)
L7 - 20°C (pre-melt)
L7 - 90°C
L7 - 20°C (post melt)
(8)
L8 - 20°C (pre-melt)
L8 - 90°C
L8 - 20°C (post melt)
(9)
L9 - 20°C (pre-melt)
L9 - 90°C
L9 - 20°C (post melt)
(10)
L10 - 20°C (pre-melt)
L10 - 90°C
L10 - 20°C (post melt)
(11)
L11 - 20°C (pre-melt)
L11 - 90°C
L11 - 20°C (post melt)
(12)
L12 - 20°C (pre-melt)
L12 - 90°C
L12 - 20°C (post melt)
(13)
L13 - 20°C (pre-melt)
L13 - 90°C
L13 - 20°C (post melt)
(14)
L14 - 20°C (pre-melt)
L14 - 90°C
L14 - 20°C (post melt)
(15)
L15 - 20°C (pre-melt)
L15 - 90°C
L15 - 20°C (post melt)
(16)
L16 - 20°C (pre-melt)
L16 - 90°C
L16 - 20°C (post melt)
MRE
Wavelength (nm)

Figure S6

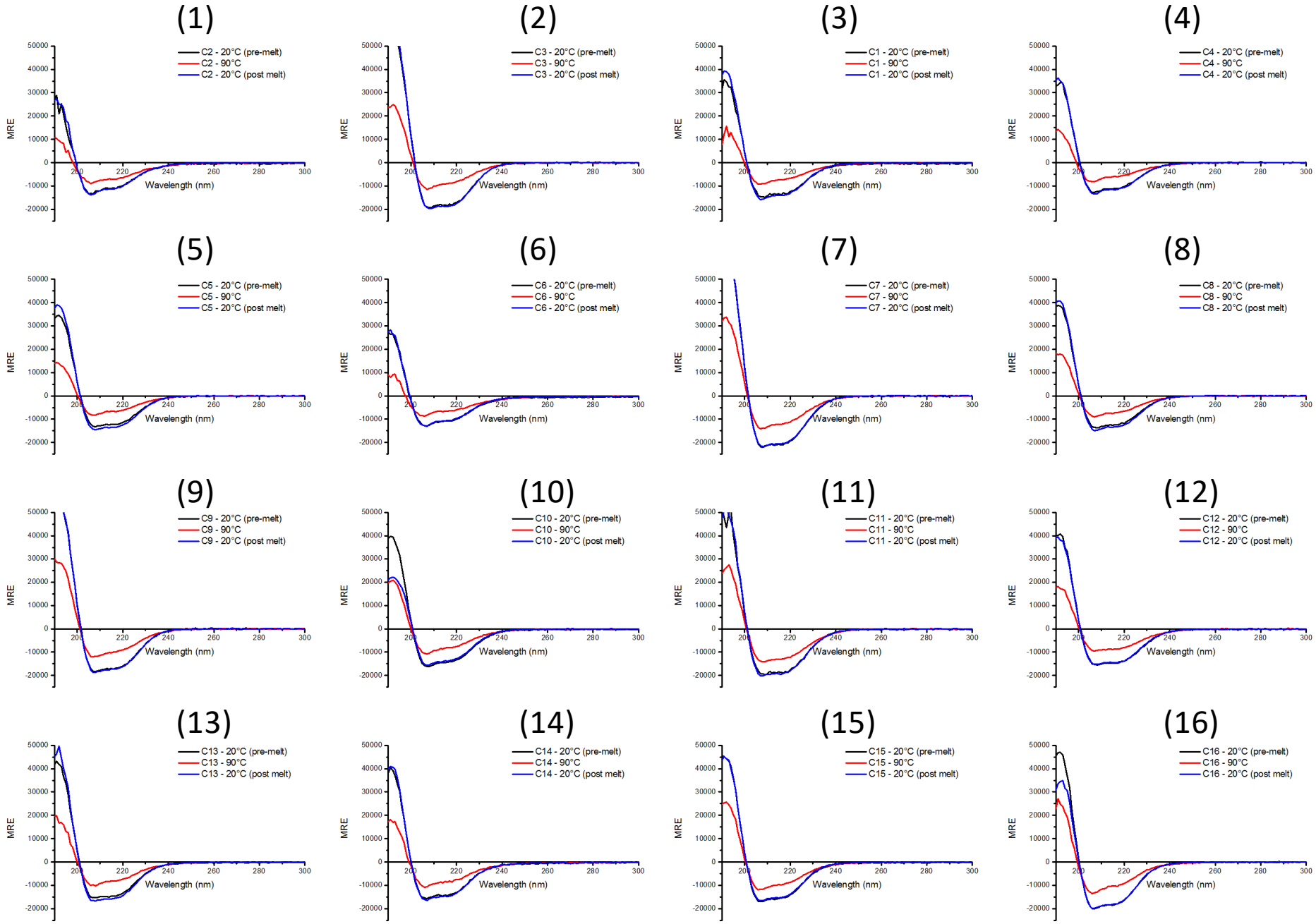
(1)
C2 - 20°C (pre-melt)
C2 - 90°C
C2 - 20°C (post melt)
(2)
C3 - 20°C (pre-melt)
C3 - 90°C
C3 - 20°C (post melt)
(3)
C1 - 20°C (pre-melt)
C1 - 90°C
C1 - 20°C (post melt)
(4)
C4 - 20°C (pre-melt)
C4 - 90°C
C4 - 20°C (post melt)
(5)
C5 - 20°C (pre-melt)
C5 - 90°C
C5 - 20°C (post melt)
(6)
C6 - 20°C (pre-melt)
C6 - 90°C
C6 - 20°C (post melt)
(7)
C7 - 20°C (pre-melt)
C7 - 90°C
C7 - 20°C (post melt)
(8)
C8 - 20°C (pre-melt)
C8 - 90°C
C8 - 20°C (post melt)
(9)
C9 - 20°C (pre-melt)
C9 - 90°C
C9 - 20°C (post melt)
(10)
C10 - 20°C (pre-melt)
C10 - 90°C
C10 - 20°C (post melt)
(11)
C11 - 20°C (pre-melt)
C11 - 90°C
C11 - 20°C (post melt)
(12)
C12 - 20°C (pre-melt)
C12 - 90°C
C12 - 20°C (post melt)
(13)
C13 - 20°C (pre-melt)
C13 - 90°C
C13 - 20°C (post melt)
(14)
C14 - 20°C (pre-melt)
C14 - 90°C
C14 - 20°C (post melt)
(15)
C15 - 20°C (pre-melt)
C15 - 90°C
C15 - 20°C (post melt)
(16)
C16 - 20°C (pre-melt)
C16 - 90°C
C16 - 20°C (post melt)
MRE
Wavelength (nm)

Figure S7

(A)

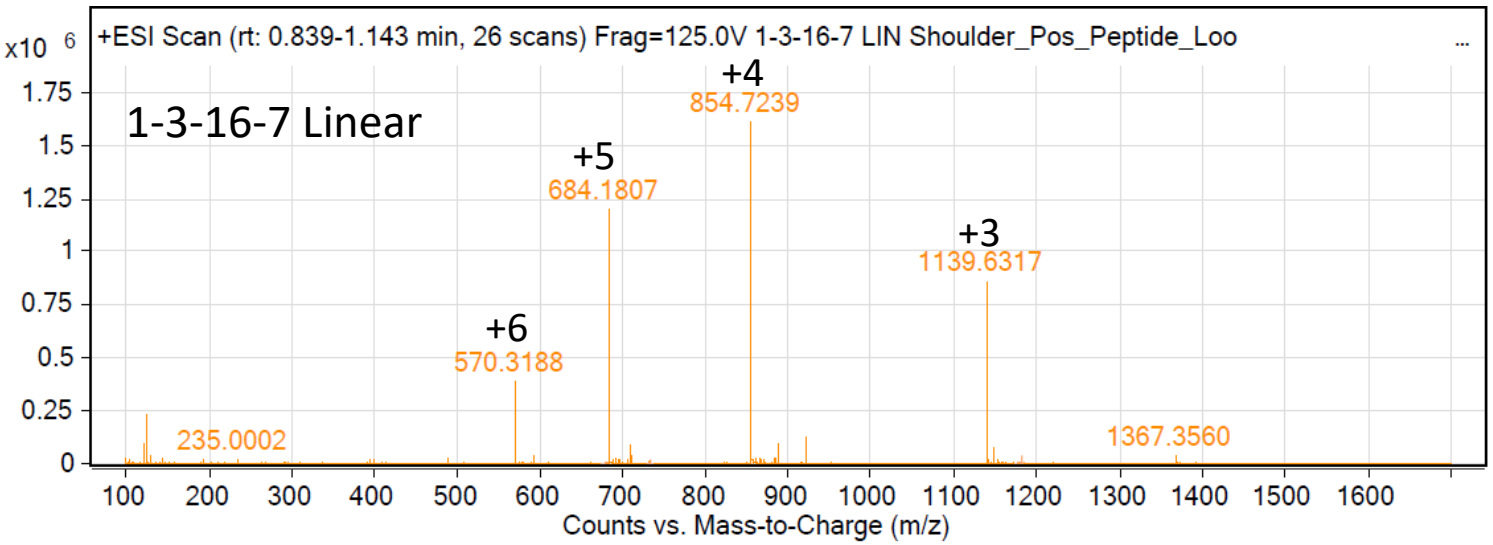
+ESI Scan (rt: 0.839-1.143 min, 26 scans) Frag=125.0V 1-3-16-7 LIN Shoulder_Pos_Peptide_Loo
x10 6
1.75
1.5
1.25
1
0.75
0.5
0.25
0
1-3-16-7 Linear
+4
854.7239
+5
684.1807
+3
1139.6317
+6
570.3188
235.0002
1367.3560
100 200 300 400 500 600 700 800 900 1000 1100 1200 1300 1400 1500 1600
Counts vs. Mass-to-Charge (m/z)

(B)

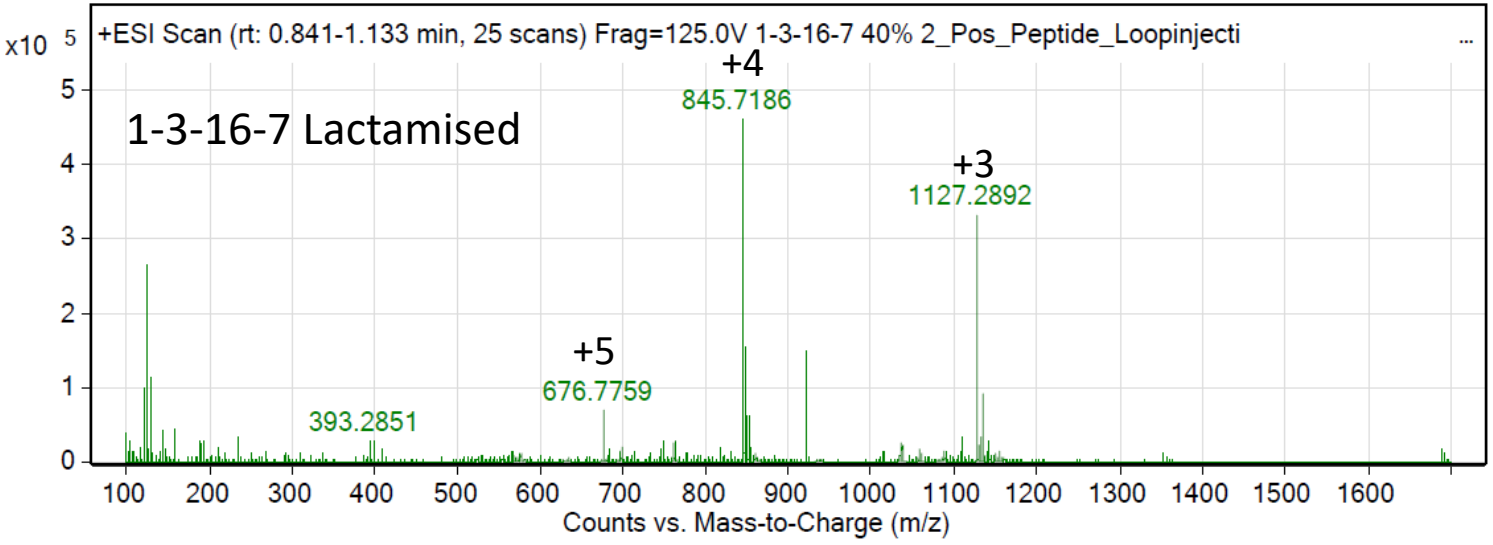
+ESI Scan (rt: 0.841-1.133 min, 25 scans) Frag=125.0V 1-3-16-7 40% 2_Pos_Peptide_Loopinjecti
x10 5
5
4
3
2
1
0
1-3-16-7 Lactamised
+4
845.7186
+3
1127.2892
+5
676.7759
393.2851
100 200 300 400 500 600 700 800 900 1000 1100 1200 1300 1400 1500 1600
Counts vs. Mass-to-Charge (m/z)

Figure S8

(A)

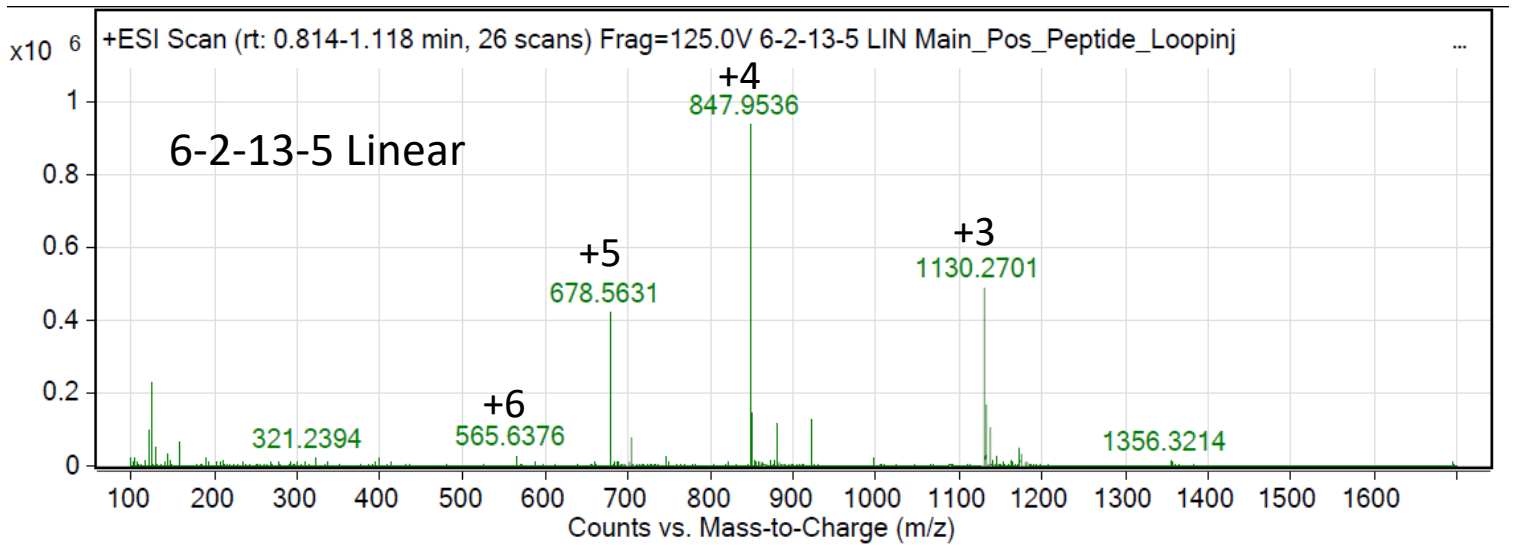
+ESI Scan (rt: 0.814-1.118 min, 26 scans) Frag=125.0V 6-2-13-5 LIN Main_Pos_Peptide_Loopinj
x10 6
6-2-13-5 Linear
+4
847.9536
+5
678.5631
+3
1130.2701
+6
565.6376
321.2394
1356.3214
Counts vs. Mass-to-Charge (m/z)

(B)

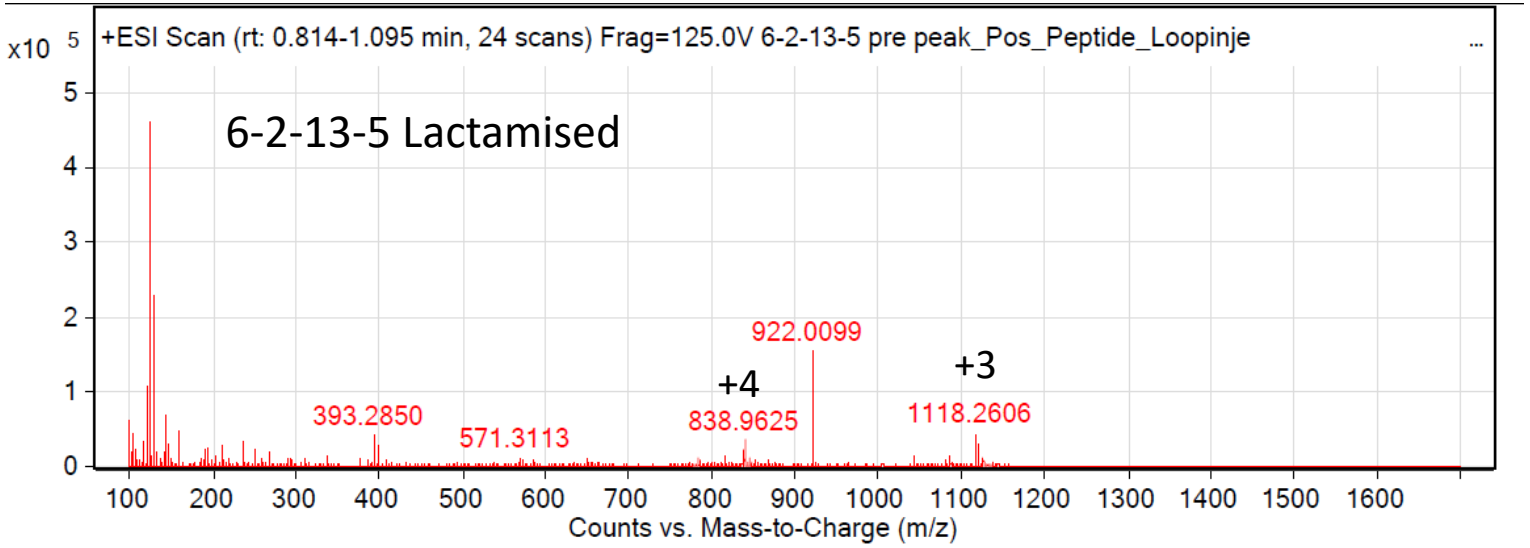
+ESI Scan (rt: 0.814-1.095 min, 24 scans) Frag=125.0V 6-2-13-5 pre peak_Pos_Peptide_Loopinje
x10 5
6-2-13-5 Lactamised
922.0099
+4
838.9625
+3
1118.2606
393.2850
571.3113
Counts vs. Mass-to-Charge (m/z)